ATAD3 is a limiting factor in mitochondrial biogenesis and adipogenesis of white adipocyte-like 3T3-L1 cells

Shuijie Li, Rui Xu, Yao Yao, Denis Rousseau

Received: 11 January 2024 | Revised: 3 June 2024 | Accepted: 3 June 2024

DOI: 10.1002/cbin.12206

RESEARCH ARTICLE

Cell Biology International WILEY

ATAD3 is a limiting factor in mitochondrial biogenesis and adipogenesis of white adipocyte-like 3T3-L1 cells

Shuijie Li[1] | Rui Xu[2] | Yao Yao[2] | Denis Rousseau[1,3]

[1]Department of Biology, University Grenoble Alpes, Grenoble, France

[2]Institute of Biochemistry and Cell Biology of Shanghai Institutes for Biological Sciences Chinese Academy of Sciences, Shanghai, China

[3]Laboratoire des Matériaux et du Génie Physique–Interfaces entre Matériaux et Matière Biologique –Institut National Polytechnique–Centre National de la Recherche Scientifique - Unité Mixte de Recherche, Grenoble, France

Correspondence
Denis Rousseau, Laboratoire des Matériaux et du Génie Physique–Interfaces entre Matériaux et Matière Biologique–Institut National Polytechnique–Centre National de la Recherche Scientifique - Unité Mixte de Recherche, 3, parvis Louis Néel BP257, 38041 Grenoble, France.
Email: Denis.Rousseau@univ-grenoble-alpes.fr

Abstract

ATAD3 is a vital ATPase of the inner mitochondrial membrane of pluri-cellular eukaryotes, with largely unknown functions but early required for organism development as necessary for mitochondrial biogenesis. ATAD3 knock-down in *C. elegans* inhibits at first the development of adipocyte-like intestinal tissue so we used mouse adipocyte model 3T3-L1 cells to analyze ATAD3 functions during adipogenesis and lipogenesis in a mammalian model. ATAD3 function was studied by stable and transient modulation of ATAD3 expression in adipogenesis- induced 3T3-L1 cells using Knock-Down and overexpression strategies, exploring different steps of adipocyte differentiation and lipogenesis. We show that (i) an increase in ATAD3 is preceding differentiation-induced mitochondrial biogenesis; (ii) down-regulation of ATAD3 inhibits adipogenesis, lipogenesis, and impedes overexpression of many mitochondrial proteins; (iii) ATAD3 re-expression rescues the phenotype of ATAD3 KD, and (iv) differentiation and lipogenesis are accelerated by ATAD3 overexpression, but inhibited by expression of a dominant-negative mutant. We further show that the ATAD3 KD phenotype is not due to altered insulin signal but involves a limitation of mitochondrial biogenesis linked to Drp1. These results demonstrate that ATAD3 is limiting for in vitro mitochondrial biogenesis and adipogenesis/lipogenesis and therefore that ATAD3 mutation/over- or under-expression could be involved in adipogenic and lipogenic pathologies.

KEYWORDS
3T3-L1 cells, ACC, adipocyte, AMPK, ATAD3, Drp1

1 | INTRODUCTION

Mitochondria are at the crossroad of many anabolic and catabolic pathways and much more than a main cellular ATP supplier. Among the many other functions, they are also a key player in lipid metabolism. They are well known for their role in lipolysis via β-oxidation, but they also contribute to lipogenesis and lipid storage in adipocytes and other tissues (Frayn et al., 2006; Goodman, 2008; Kazantzis & Stahl, 2012; Novikoff et al., 1980; Walther & Farese, 2009) and to biogenesis of membrane phospholipids like phosphatidylethanolamine, phosphatidylcholine or cardiolipin (Epand et al., 2007; Vance, 2008; Voelker, 2003). Mitochondria are also essential for the conversion of cholesterol, for example, the synthesis of steroids in endocrine cells, (Miller, 2011) and

require themselves lipid import for their biogenesis. Within the cell, mitochondria are tethered to the endoplasmic reticulum (ER) (de Brito & Scorrano, 2008) thus allowing among others lipid trafficking, local calcium signaling (Csordás et al., 2006; Goetz et al., 2007; Szabadkai et al., 2006; Wang et al., 2000) and translocation of nuclear-encoded mitochondrial proteins (de Brito & Scorrano, 2010). Finally, mitochondria are dynamic as they are able to divide and fuse, move and dock or die, according to specific mitochondrial and cellular conditions like e.g. cell growth or starvation (Kageyama et al., 2011; Osman et al., 2011; Westermann, 2010). Consequently, dysregulation of mitochondrial activities gives rise to many otherwise unrelated pathologies such as myopathies, neuropathies, cardiopathies, obesity, diabetes and some others like cancers (Campello & Scorrano, 2010; Choo et al., 2006). ATAD3 was discovered in 2003 as gene target of c-Myc (Frayn et al., 2006; Zeller et al., 2003). Although *in silico* analysis reveals an ATPase domain, its true physiological function is still unknown although many functions have been shown to be linked to ATAD3 (Arguello et al., 2021; Baudier, 2018; Lee & Kim, 2022; Peralta et al., 2018; Shu et al., 2021). ATAD3 is present in all pluricellular organisms as a single gene and further evolved in primates into three ATAD3 encoding genes present in hominidae (Li & Rousseau, 2012a). ATAD3 protein is overexpressed in patients with carcinoma (Gires et al., 2004; Schaffrik et al., 2006) and is related to cancer initiation and progression as well as to chemoresistance and apoptosis (Chen et al., 2011; Fang et al., 2010; Gires et al., 2004; Huang et al., 2011; Hubstenberger et al., 2008). The localization of ATAD3 is mitochondrial (Li & Rousseau, 2012a) and proteomic approaches identified ATAD3 as a protein of the inner membrane (Da Cruz & Martinou, 2008; Da Cruz et al., 2003). More detailed analysis revealed the topology of ATAD3 membrane insertion and its polymeric structure (Bogenhagen et al., 2008; Gilquin et al., 2010a; Hubstenberger et al., 2010; Li & Rousseau, 2012a). ATAD3 presents a C-terminal half, corresponding to the ATPase core domain, which locates inside the mitochondrial matrix, and a specific N-terminal half located in the intermembrane space and potentially interacting with the outer membrane and cytoplasmic partners. No intrinsic ATPase activity could be identified so far, although ATAD3 has been purified as full length protein (Li et al., 2012b). Chow and colleagues have shown a possible interaction of ATAD3 with the proteins at contact sites between mitochondria and ER, like Mfn2 and dynamin-related protein 1 (Drp1 (Chiang et al., 2012);) and this may reflect a functional role of ATAD3 in biochemical communication between ER and mitochondria (Gilquin et al., 2010b). More is known about the role of ATAD3 at the cellular and organ level. ATAD3 is essential for early embryogenesis of *Caenorhabditis elegans*, (Hoffmann et al., 2009; Kamath, 2003; Piano et al., 2002; Simmer et al., 2003; Sonnichsen et al., 2005) *Drosophila melanogaster*, (Gilquin et al., 2010b; Guertin et al., 2006) and *Mus musculus* (Goller et al., 2013). Although, ATAD3 is expressed in all tissues and cells studied so far, the knockdown of ATAD3 in *C. elegans* primarily affects the intestinal fat tissue and the gonads at a time when these cells have to initiate mitochondrial biogenesis and lipogenesis (Walther & Farese, 2009). Because in worm the intestinal cells are the functional equivalent of white adipocytes, (McKay et al., 2003) 3T3-L1 murine cells can be used as a well-accepted and extensively studied mammalian model to analyze molecular processes associated with adipocyte differentiation and lipid storage. Upon induction with insulin, dexamethasone and isobutylmethyl-xanthine, these cells undergo a complete differentiation into adipocytes, acquiring the capacity for massive lipogenesis. These processes are characterized by a significant mitochondrial mass increase that just precedes lipid storage (Gao et al., 2011; Kita et al., 2009; Wilson-Fritch et al., 2003). Mitochondrial biogenesis-linked lipogenesis has been also observed in humans (Bogacka et al., 2005; Kaaman et al., 2007). Mitochondrial biogenesis may be linked to lipid storage by (i) ATP supporting metabolic processes involved in lipid storage and/or (ii) mitochondrial export of acetyl-CoA (or citrate transformed into acetyl-CoA by the ATP citrate lyase), which is then metabolized into malonyl-CoA by the acetyl-CoA carboxylase (ACC), a precursor of triacylglycerol that is ultimately forming lipid droplets (Guo et al., 2009; Kajimoto et al., 2005; Muoio et al., 1999; Shi & Burn, 2004). Lipid droplets become coated with a monolayer of phospholipids 94 and a set of proteins (Perilipin) that stabilizes them within the cytoplasm (Blanchette-Mackie et al., 1995). Electron microscopy studies have detailed the spatial organization of the cellular organelles during adipogenesis/lipogenesis and have shown that mitochondria, ER and lipid droplets are closely organized, (Blanchette-Mackie et al., 1995) and that mitochondria increase in density during differentiation (Wilson-Fritch et al., 2003). Here we investigated the role of ATAD3 during adipocyte differentiation of 3T3-L1 cells by transient and stable modifications of the cellular ATAD3 level. We found that ATAD3 is overexpressed early upon induction of 3T3-L1 differentiation, at the beginning of the mitochondrial mass increase. Gradual knock-down of ATAD3 in 3T3-L1 inhibited adipocyte differentiation and lipogenesis in a correlative manner, without affecting the insulin pathway, and this phenotype could be rescued by ATAD3 re-expression. Inhibition of lipogenesis was linked to a lack of ACC overexpression and activation. It appeared to correlate with altered mitochondrial remodeling and reduced mitochondrial biogenesis, and this phenotype could be partially complemented by overexpression the mitochondrial fission protein Drp1. These results suggest an essential role of ATAD3 in mitochondrial biogenesis, necessary for terminal adipocyte differentiation and lipogenesis.

2 | MATERIALS AND METHODS

2.1 | Cells, treatments and biopsies

The mouse 3T3-L1 cells used in this study were purchased from American Type Culture Collection (ATCC). 3T3-L1 preadipocytes were cultured in a Dulbecco's Modified Eagle's Medium (DMEM, GibcoTM) containing 10% FBS (Biowest, EU) at 37℃ and 5% CO_2

until confluence and maintained for 48 h (Day 0). Cells were induced to differentiate using MDI induction medium (DMEM containing 10% FBS and 0.5 mM 3-isobutyl-1- methylxanthine, 1 µM dexamethasone, and 1 µM insulin) for 2 days, followed by insulin medium (DMEM containing 10% FBS and 1 µM insulin) for 2 days. The medium was subsequently replaced with fresh culture medium (DMEM with 10% FBS) containing insulin (1 µM) every 2 days until the terminal differentiation. Adipose tissues were taken from C57Bl6 male mice according to ethic rules (animal experimentation certificate 380537). Cell numbers were determined by manual counting of the cells under microscope. Data presented in this work (if not mentioned otherwise) are normalized to cell number, since expression of almost all proteins increased along the differentiation process, including actin, considered constitutive and often used for normalization (e.g., Figure 3b).

2.2 | ShRNA stable cell lines

For the stable ATAD3 knockdown cells, a retrovirus-based siRNA expression system was used. The sequences of ATAD3 were 223, 5′-GGACAAATGGAGCAACTTC; 354, 5′-GAACAGCAGTCCAAGCTCA; 530, 5′- ACAACAGCAACTTCTGAAT; 1084, 5′- GCCATCGCAACAAGAAATA; and 1791, 5′- GCAGAAGATGCAGTGGCTT, and cloned into a pSIREN-Retro-Q Vector and shuttled into Knockout RNAi Systems (Clontech Laboratories Inc). A control sequence, 50-AACTAGAGCCACAACTACC-3′, was used as control. The retrovirus was produced in HEK293 cell following the manufacturer's protocol and infected the proliferating 3T3-L1 cells. The stable cell lines were selected in medium supplemented 136 with 5 µg/mL of puromycin. Sequences of siRNA are presented in Supporting Information S8: Table S1.

2.3 | Confocal microscopy

Cells were seeded in the Lab-TekTM-Chamber slide system (Nunc) and induced to differentiate for various time periods. Just before imaging, cells were incubated with 200 nM MitoTraker Green FM (Interchim) at 37°C in a 5% CO_2 incubator for 30 min and 1 µg/mL Hoechst 33342 in the dark at 37°C for 10 min. After staining, cells were washed twice with prewarmed phosphate-buffered saline (PBS), and fresh DMEM medium was added. Images were collected with a Leica TCS SP2 AOBS inverted laser scanning confocal microscope equipped with a 63× water immersion objective (HCX PL APO 63.0×/1.40 W Corr). Laser excitation was 351–364 nm for Hoechst and 488 nm for Mito-Tracker Green. Fluorescence emissions adjusted with AOBS were 390–470 nm for Hoechst and 498–549 nm for MitoTracker Green. 3D images of mitochondria were acquired by at least 10 optical sections of 1µm z-step. Analysis and quantification of mitochondrial skeleton was processed using ImageJ software.

2.4 | Electron microscopy

Cells adherents to the coverslip were fixed with 2.5% glutaraldehyde in 0.1 M cacodylate buffer pH 7.4 during 2 h at room temperature. Cells were then washed with buffer and postfixed with 2% Osmium tetroxyde in the same buffer during 1 h at 4°C. After extensive washing with distilled water, cells were stained with 1% uranyl acetate pH 4 during 1 h at 4°C. Cells were then dehydrated through a graded series of alcohol concentrations (30%–60%–90%–100%–100%–100%) and infiltrated with a mix of 1/1 Epon/alcohol 100% during 1 h before several baths in fresh Epon (Fluka) during 3 h. Finally, a capsule full of Epon was deposed on the surface of the cells and the resin was let to polymerize during 72 h at 60°C. The polymerized bloc was then detached from the culture cover-slip with hydrofluoric acid 48% during 1 h at room temperature 161 and ultrathin sections of the cell monolayer were cut with an ultramicrotome (Leica). Sections were post-stained with 4% Uranile acetate and 0.4% lead citrate before being observed in an electron microscope at 80 kV (JEOL 1200EX). Images were acquired with a digital camera (Veleta, SIS, Olympus) and morphometric analysis was performed with iTEM software (Olympus).

2.5 | Oil-Red-O staining

Cells were washed twice with PBS and fixed with 4% paraformaldehyde in PBS for 30 min at room temperature. After fixation, cells were washed two times with distilled water and one time with 60% isopropanol. The plates were dried for 30 min at room temperature and then cells were stained with filtered Oil-Red-O working solution (stock solution: 3 mg/mL in isopropanol; working solution: 60% Oil-Red-O stock solution and 40% distilled water) for 10 min at room temperature, washed four times with distilled water, and plates were dried and scanned for images. Oil-Red-O dye was extracted using 100% isopropyl alcohol and measured by spectrophotometry at 500 nm. Plastic well staining background was subtracted, and data normalized to the staining of pre-adipocytes (Day 0) set to a value of one.

2.6 | Western blot analysis

The 3T3-L1 wild-type and the three siRNA cell lines were propagated in duplicate in 6-well plates. Proteins were extracted, at various time points, in Laemmli buffer containing 10 mM DTT and 5% 2-mercaptoethanol. Samples (containing same cell amount) were separated by 10% SDS-PAGE and electro-blotted onto nitrocellulose membrane. The nitrocellulose membranes were incubated for 1 h at room temperature with blocking buffer containing TBST (Tris-buffered saline (25 mM Tris), 0.1% Tween 20) complemented with 3% nonfat dry milk powder, further incubated at 4°C overnight with

primary antibodies in blocking buffer, washed three times for 10 min each with TBST at room temperature, and finally incubated at room temperature for 1 h with secondary 187 antibodies in blocking buffer. After washing three times for 10 min each in TBST, detection was performed by enhanced chemiluminescence (ECL Plus, GE Healthcare). Primary rabbit polyclonal antibodies (all from Cell Signaling Technology and used at 1:1000 dilution unless stated otherwise) were directed against: phospho-ACC (Ser79), ACC, phospho-Akt (Thr308), Akt (Santa Cruz), phospho-mTOR (Ser2448), mTOR, 4EBP1, phospho-4EBP1 (Ser65), phospho- S6K (Thr389), S6K, phospho-AMPKα (Thr172, BD Biosciences), AMPK α, β-tubulin (Santa Cruz), β-actin (Santa Cruz), and Drp1 (Santa Cruz). Mouse monoclonal antibodies were directed against: Glut4 (Cell Signaling), Leptin (Peprotech), NRF1 (Enogene), Myc (Abcam, to detect myc-tagged Mfn2), ANT 1/2 (Santa Cruz), VDAC 1 (Santa Cruz), AK2 (ABGENT), cytochrome C (BD Biosciences), $MTCO_2$ (Santa Cruz), NDUFA10 (Santa Cruz), and finally (as part of the MitoProfile OXPHOS set, MitoScience) ATP5A (ATP synthase F1 complex, subunit 1), UQCRC2 (cytochrome b/c complex, subunit 2), MTCO1 (cytochrome oxydase, subunit 1), SDHB (succinate deshydrogenase) and NDUFB8 (NADH deshydrogenase, subunit 8). ATAD3 was detected using rabbit polyclonal antibodies raised against a specific sequence of ATAD3 (Anti-Nter: R40PAPKDKWSNFDPTG53 in ATAD3As; produced by Eurogenetec) and used as purifed immunoglobulins. Secondary antibodies were anti-mouse or anti-rabbit IgG-horse radish peroxidase conjugate (GE Healthcare). The membranes were occasionally incubated with TBST blocking buffer again with sodium azide for irreversible inactivation of HRP and re-probed with anti-β-actin and anti-β-tubulin antibodies as a loading control. Exposed films were analyzed and quantified using ImageJ (NIH).

All the Western-blots presented here were performed two or three times.

2.7 | Citrate synthase activity measurements

The reduction of 5′,5′-dithiobis (2-nitrobenzoic acid) by citrate synthase at 412 nm (extinction coefficient 13.6 mM^{-1} cm^{-1}) was followed in a coupled reaction with coenzyme A and oxaloacetate. A reaction 212 mixture of 150 mM Tris-HCl, pH 8.0, 5 mM acetyl-coenzyme A, 3 mM DTNB and 20 µL of cells lysates were incubated at 37°C for 5 min. The reaction was initiated by the addition of 0.5 mM oxaloacetate and the absorbance changes were monitored for 5 min. All assays were normalized to cell amount by Western blot quantification of tubulin and compared to tubulin levels at Day 0.

2.8 | Measurement of mitochondrial cytochrome aa3 content

Cell samples were solubilized with 1% of sodium deoxycholate in phosphate buffer (KH2PO4 100 mM, pH8). The differential absorbance spectrum of reduced (by dithionite) versus oxidized cytochromes was obtained by scanning from 400 to 650 nm using a Cary50 Bio spectrophotometer (Varian). Cytochromes of the respiratory chain were reduced by addition of sodium dithionite crystals to 1 mL of suspension (final concentration of 0.25 mg/mL). Absorbance at 605 nm was used for quantification of respiratory chain cytochrome aa3 (constituent of cytochrome c oxydase) with extinction coefficient 24 $mM^{-1}cm^{-1}$ (Monge et al., 2008).

2.9 | Transient transfection of siRNA and plasmids

RNA interference was used for transient downregulation of ATAD3. The sequences of double stranded RNAs for ATAD3 were: Sequence 1: Forward 5′-ACAACAGCAACUUCUGAAUdTdT-3′, Reverse 3′-dTdTUGUUGUCGUUGAAGACUUA-5′ Sequence 2: Forward 5′-ACAGCAGUCCAAGCUCAAGdTdT-3′ Reverse 3′-dTdTUGUC GUCAGGUUCGAGUUC-5′ Plasmid encoding mouse ATAD3 is pCDNA3.1+ based; Drp1- and Mfn2-Myc-encoding plasmids are respectively P26048 and P23213 pCDNA3-based from Addgene. For transient transfection, wild-type 3T3-L1 preadipocytes cultured in 6-well plates and induced to differentiate for 2 days were transfected once with 50 nM dsRNAs or twice 237 with 10 µg of plasmid DNA (differentiation Days 2 and 3) using Lipofectamine 2000 (Invitrogen) according to the manufacturer's protocol. After 6 h, the transfection medium was replaced with DMEM containing 10% FBS. The samples for Western blot were collected at Day 6 (siRNA) or Day 8 (plasmids). The cells prepared for the Oil-Red-O coloration were maintained and replaced with insulin medium (DMEM containing 10% FBS and 1 µM insulin) until terminal differentiation (Days 8–12). For the stable transfection, wild-type and siRNA knock-down 3T3-L1 preadipocytes cultured in dishes were transfected with 5 µg/mL of plasmids encoding ATAD3, Drp1 and Myc-tagged Mfn2 using Lipofectamine 2000 (Invitrogen). 72 h posttransfection, cells were selected with antibiotic G418 (750 µg/ml) during 2–3 weeks with medium replaced every 2 days. Selected cells were grown as pools. For stable re-expression of ATAD3, we used an untagged ATAD3 expression plasmid because the rescue efficiency of a C-terminally Myc-tagged expression plasmid was very low.

2.10 | Oxymetry

Wild-type and siRNA 3T3-L1 preadipocytes were isolated by free Ca2+ Mitomed solution (0.5 mM EGTA, 95.21 mM MgCl2, 60 mM K-lactobionate, 20 mM taurine, 3 mM KH2PO4, 20 mM HEPES, 110 mM sucrose, 0.5 mM DTT). A standardized number of cells (106) was permeabilized with saponin (25 µg/mL) and the rates of oxygen consumption (nMole O2/cell/min) were determined with high-resolution respirometry (oxygraph-2K, OROBOROS Instruments) in Mitomed solution. Measurements were carried out by sequential addition of (final concentrations given): 5 mM glutamate/2 mM malate as complex I substrates (v0 Glu/Mal, state IV respiration), 2 mM ADP for maximal respiration (vmax Glu/Mal, state

III respiration), 3 µM rotenone to inhibit complex I, and finally 10 mM succinate as complex II substrate (Vmax succinate, state III respiration). All measurements were carried out at 25°C and the solubility of oxygen was taken as 240 nmol. Oxygen consumption is expressed in nM of 02/cell/min and Respiratory Indexes indicated in the text for glutamate/malate are vmax/v0 ratios.

2.11 | Quantitative RT-PCR

Total RNA was extracted from 3T3-L1 cells with Trizol (Invitrogen). First- strand cDNAs were synthesized from 1 µg of total RNA in the presence of the PrimeScript RT Enzyme Mix (Takara), using a mixture of random examers and Oligo(dT) primers (Promega). Real-time PCR assays were performed using a Rotor-Gene Q (Qiagen). TATA box-binding protein mRNA level was used to normalize the data. PCR primer sequences are listed in Supporting Information S8: Table S2.

2.12 | Adenylate nucleotides

ATP, ADP, and AMP were determined in protein-free extracts prepared as follows. Cell lysis and protein precipitation were performed directly in culture flasks. Cells were washed 3 times with PBS, and ice-cold 0.6 N perchloric acid was added to lyse cells and precipitate proteins. Precipitated material was removed by centrifugation (2 min, 15,500 × *g*, 4°C). The supernatant was neutralized with KOMO (KOH 2 N, MOPS 0.3 M) and precipitate formed during neutralization was removed by centrifugation (10 min, 15,500 × *g*, 4°C). Supernatants were stored at −80°C and used for HPLC-based nucleotide quantification as described (Gratia et al., 2012).

2.13 | Statistics

Experiments were repeated at least three times and mostly analyzed in different parallels. Resulting data are given as means +/− standard deviation. Differences between data were analyzed by two-tailed, two-sample, unequal-variance Student's *t* test with *p*-levels indicated according to * for $p < .05$, ** for $p < .01$, *** for $p < .001$.

3 | RESULTS

3.1 | Adipogenesis and lipogenesis correlate with changes in mitochondrial mass and function, and early ATAD3 upregulation

Mouse 3T3-L1 preadipocyte cells were induced by insulin to differentiate into adipocytes, that is, to undergo adipogenesis and lipogenesis. This activated the canonical Akt signaling (Figure 1a) and led to an about threefold increase in the cellular protein content (Figure 1b). We characterized this differentiation process, lasting until Days 10–12, in respect to mitochondrial structure and function, as well as to expression of ATAD3 and other mitochondrial proteins. The mitochondrial network of 3T3-L1 cells underwent a strong remodeling process during the course of differentiation (Figure 1c) as observed also by others (Blanchette-Mackie et al., 1995; Kita et al., 2009; Wilson-Fritch et al., 2003). Starting around days 3-4 and until terminal differentiation around Days 10–12, the mitochondrial mass increased, as observed qualitatively by elevated Mitotracker staining (Figure 1c and Supporting Information S1: Figure S1) and quantitatively by the measurement of mitochondrial citrate synthase activity (12-fold increase, Figure 1d) and cytochrome aa3 absorbance (11-fold increase, Supporting Information S2: Figure S2A,B). These latter parameters, like most data presented in this work (if not mentioned otherwise) were normalized to cell number. As compared to Mitotracker, these measures are also less likely perturbed by lipid-induced quenching. A similar increase of the mitochondrial mass during 3T3-L1 differentiation was suggested by a sixfold increase in mtDNA copy number (Gao et al., 2011). Tracing of the mitochondrial network during 3T3-L1 differentiation by confocal 3D-analysis (Figure 1c,e) revealed a transient reticulation of the network occurring until Day 6, followed by the onset of a fragmentation process until Day 12. These structural mitochondrial changes were confirmed by electron microscopy observations, showing in the differentiated state more numerous and less elongated mitochondria (from 1.25 µm in mean to 0.9 µm) that were located close to ER- associated lipid droplets (Figure 1f and Supporting Information S2: S2C,F). Triglyceride accumulation as quantified by Oil-Red-O staining showed onset of lipogenesis at around Days 2–4 of differentiation (Figure 1g). Thus, mitochondrial remodeling and lipid storage seem to occur concomitantly. However, there is no evidence that the change in mitochondrial ultrastructure is forced by the density of lipid droplets, since these are not yet very abundant at day 8 as compared to later time points of adipocyte differentiation.

The level of mitochondrial proteins, as evaluated by Western blot analysis, increased approximatively with the mitochondrial mass, but the exact relation depended on the protein (Figure 2a): ATAD3 showed an increase that occurred already early (Day 2) and was strong (eightfold). These ATAD3 protein levels were comparable to those of C57Bl6 mouse peritoneal adipose tissue (Figure 2b). Other analyzed proteins increased later and to variable degree. ACC, a rate limiting enzyme in lipid synthesis, is overexpressed along differentiation as later its phosphorylated form.

The effect of the mitochondrial mass increase and reorganization on respiration was analyzed by oxymetry in permeabilized 3T3-L1 cells at Days 0 and 8. When normalized to cell number, respiratory parameters changed only moderately with time (Figure 2c, black bars). Mitochondrial respiration showed a twofold increase of state IV with glutamate/malate and state III with succinate, while state III with glutamate/malate remained unchanged. The resulting respiratory control ratio with glutamate/malate (RCR, state III/state IV) decreased from 2.1 to only 1.1, indicating some uncoupling in the differentiated state. However, when respiration was normalized to

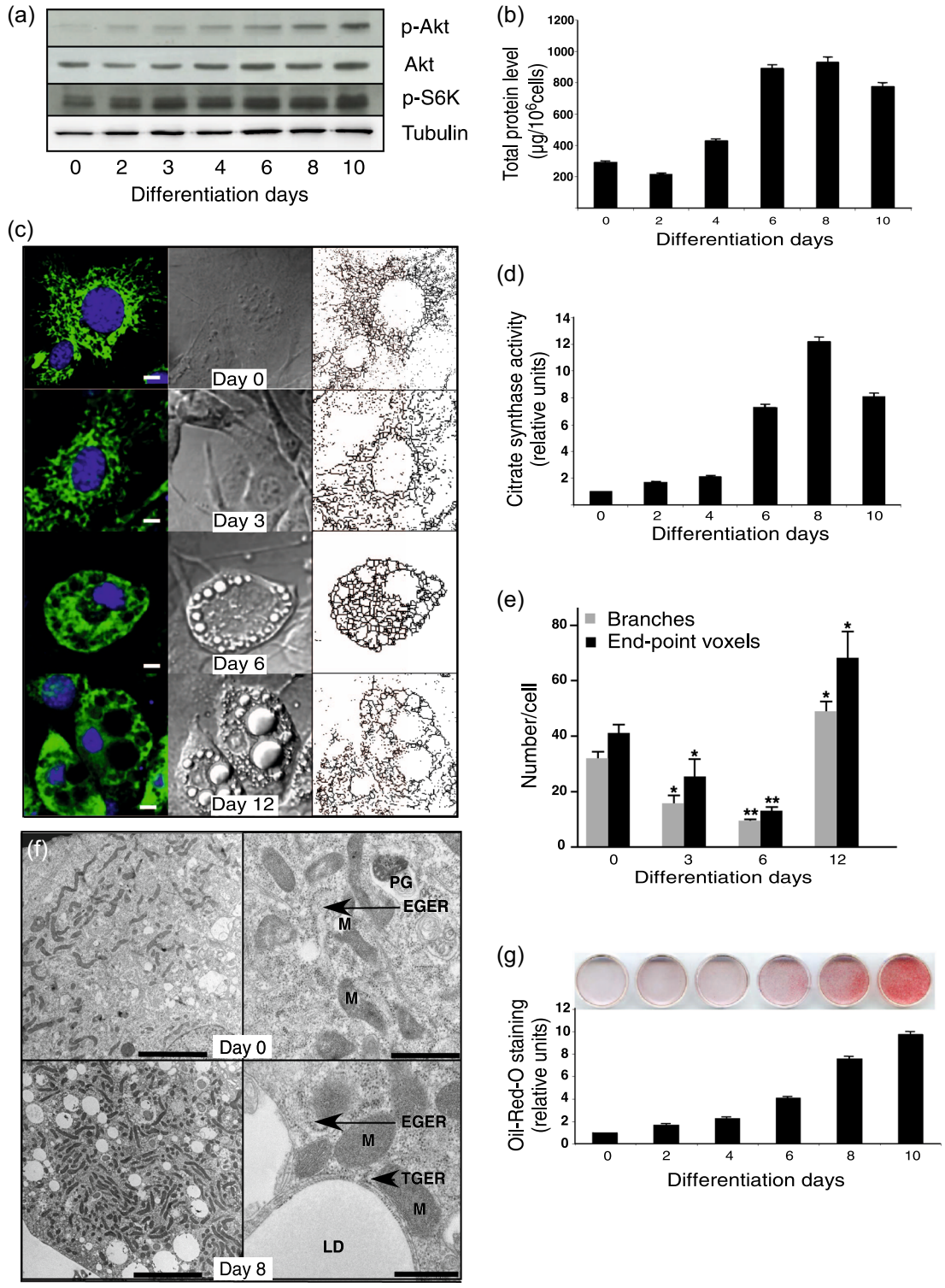

FIGURE 1 (See caption on next page).

mitochondrial mass (Figure 2d), all types of respiration were drastically reduced. Taken together, these findings suggest that mitochondrial activity during differentiation is much less devoted to respiration, and rather redirected to other metabolic activities like lipogenesis.

Triglyceride accumulation may not require so much respiration per se since Antimycin A, an inhibitor of the respiratory complex III, can induce itself lipogenesis ((Vankoningsloo et al., 2005) and Supporting Information S7: Figure S7A, with a 150% increase of lipogenesis at Day 16 with 100 nM Antimycin).

3.2 | ATAD3 knock-down inhibits lipogenesis by blocking ACC, not insulin-Akt signaling

To understand whether induction of ATAD3 expression in 3T3-L1 cells is important for the differentiation phenotype, including lipid storage and mitochondrial biogenesis and remodeling, we performed ATAD3 knock-down (KD) by stable lentiviral ATAD3-targeted siRNA expression in 3T3-L1 cells. Two cell lines with graded reduction in ATAD3 expression, intermediate (line 1084) and low (line 530), were selected for further experiments (Figure 3a and Supporting Information S3: S3A). They revealed that lowered ATAD3 level clearly correlates with reduced triglyceride accumulation, thus indicating inhibition of lipogenesis during adipocyte differentiation. A similar result was obtained in a transient ATAD3 KD model using siRNA in 3T3-L1 cells (Supporting Information S3: Figure S3B), suggesting that inhibition of lipogenesis is an early consequence of ATAD3 invalidation. Also the opposite effect was observed by transient ATAD3 overexpression (Supporting Information S3: Figure S3C). This inhibition was not due to an altered insulin-Akt signaling, since increased activation of Akt (p-Akt/total Akt ratio) is observed in all cell lines during induced-differentiation (Figure 3b). Furthermore, inhibition of differentiation in stable ATAD3 KD is neither due to a delayed response to insulin, as forced induction of differentiation using a four times higher dose of insulin for 24 days, with or without oleic acid, an inducer of adipogenesis and lipogenesis (Xie et al., 2006) could not overcome the ATAD3 KD-induced inhibition of lipogenesis (Supporting Information S3: Figure S3D). Consistent with these findings, the insulin-induced increase in cellular protein content was only moderately inhibited by about 25% in KD lines (Figure 3c), with some proteins even accumulating normally in KD lines, such as actin (Figure 3b). Therefore, the inhibition of lipogenesis induced by ATAD3 KD does not seems to be related to a disturbed action of insulin signaling. We then asked whether the observed changes in lipogenesis are controlled by acetyl-CoA carboxylase (ACC), a rate-limiting key enzyme in fatty acid synthesis and triglyceride production. ACC expression level was indeed upregulated during 3T3-L1 differentiation, to the largest extend observed among all proteins tested (Figure 3b), and this upregulation was decreased in ATAD3 KD cells. The phosphorylated form of ACC is even more increased during differentiation, leading to a decrease of pACC/ACC ratio corresponding to the activation of ACC, which is linked to increased lipogenesis. In ATAD3 KD cell lines this ACC activation is reduces as expected from the lower lipogenesis. ACC can be inhibited by phosphorylation via AMP-activated protein kinase (AMPK), a central nutrient and energy stress sensing pathway involved in the regulation of lipogenesis/lipolysis. We therefore examined whether ACC phosphorylation state could depend on AMPK activation (Figure 3b). During 3T3-L1 differentiation we observed a slight decrease of the AMPK phosphorylation state (p-AMPK/total AMPK ratio, Figure 3b), and this observation is the same in KD lines.

Allosteric activation of AMPK via cellular ADP/ATP or AMP/ATP ratios (Hardie et al., 2012; Suter et al., 2006) was neither decreased in WT versus KD cells (Supporting Information S3: Figure S3E). Rather the opposite was observed, namely a transient increase in these ratios in WT cells at differentiation Day 4, indicative for energy stress at the onset of massive lipogenesis. In conclusion, stable ATAD3 KD partially blocks ACC overexpression and activation (lowering of phosphorylation state) after insulin-induction, and such a regulation is entirely consistent with observed lipogenesis inhibition (Figure 3a). However, stable ATAD3 KD has no significant effect on AMPK activation, and changes in ACC phosphorylation state may rather be a consequence of the large differences in ACC expression, and/or unknown ACC dephosphorylation steps.

Since cellular KD models suggest ATAD3 as a potent limiting factor in mitochondrial remodeling, adipocyte differentiation and lipogenesis, we investigated the expression of several transcriptional

FIGURE 1 Evolution of the mitochondrial network and of lipogenesis during insulin- induced differentiation of 3T3-L1 cells. (a) Expression levels of Akt pathway signaling proteins were determined during the time course of differentiation. (b) Total cellular protein per 10^6 cells was quantified by Bradford assays during the time course of differentiation. Values are given as mean +/− SD from three independent experiments ($n = 9$), with a significant difference ($p < .001$) as compared to Day 0 occurring from Day 2 onwards. (c) Mitochondrial morphology was analyzed in cells induced for differentiation and visualized by confocal microscopy imaging during the first 12 days of differentiation. Confocal images (left column) showing typical cells stained for mitochondria (green, Mitotracker GreenFM™) and nuclei (blue, Hoechst DNA staining) as are given together with phase contrast images (middle column) and the 3D-reconstituted mitochondrial network (right column). Scale bars represent 5 µm. Images of wide microscopic fields are presented in Supporting Information S1: Figure S1. (d) Quantification of citrate synthase activity along 3T3-L1 differentiation. Values are given as mean +/− SD from three independent experiments ($n = 9$), with significant difference with the control from Day 2 ($p < .001$). (e) Mitochondrial branch length and end-point voxels were quantified from confocal microscopy 3D-analysis. Values are given as mean +/− SD from three independent experiments ($n = 9$), $^*p < .05$ and $^{**}p < .01$. (f) 3T3-L1 cells were imaged by electron microscopy at Days 0 (top row) and 8 (bottom row), with increasing magnification from left to right (scale bars equal 2 and 0.5 µm). EGER, enlarged granular endoplasmic reticulum; LD, lipid droplet; M, mitochondria; PG, phagosome; TGER, tubular granular endoplasmic reticulum. Images of different microscopic fields are presented in Supporting Information S2: Figure S2D–F and mitochondria branch length measurements performed by electron microscopy 2D- analysis are presented in Supporting Information S2: Figure S2C. (g) Staining of neutral lipids of 3T3-L1 cells with Oil-Red-O during the differentiation time course. Values are given as mean +/− SD from three independent experiments ($n = 9$), with a significant difference ($p < .001$) as compared to Day 0 occurring from Day 2 onwards.

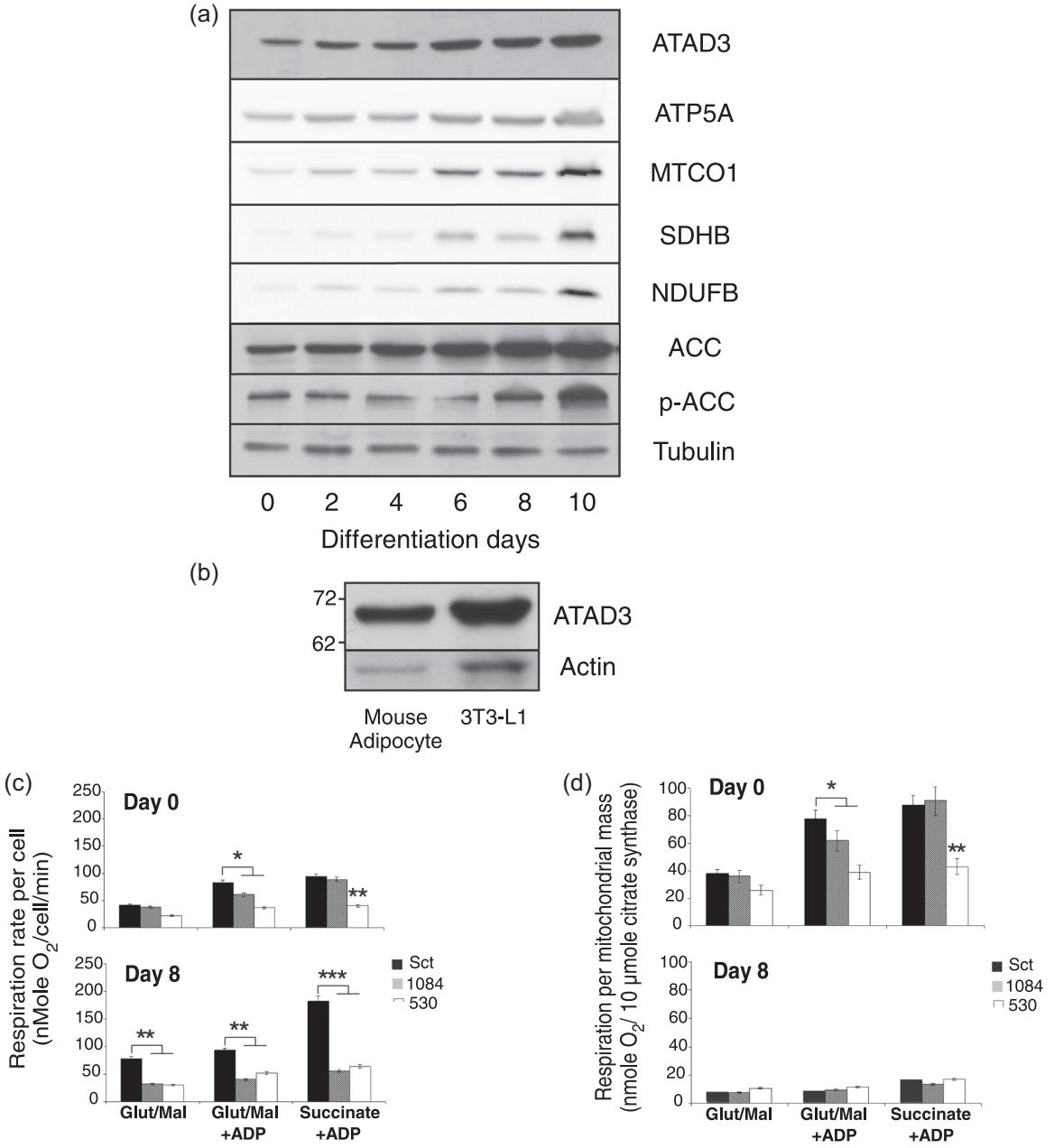

FIGURE 2 Evolution of mitochondrial proteins and respiration during insulin-induced differentiation of 3T3-L1. (a) Expression levels of ATAD3 and other mitochondrial proteins during the time course of differentiation, analyzed by Western blot analysis. Protein corresponding to equal cell number was loaded. (b) Expression levels of ATAD3 in adipocyte tissue of mice (C57Bl6) and of differentiated 3T3-L1 cells, analyzed by Western blot analysis in biopsies to demonstrate its physiological expression level. (c,d) Respiration rates of control (scrambled siRNA, SCt, black bars), and stable siRNA-ATAD3 KD cell lines 1084 (gray bars) and 530 (white bars) measured by oxymetry with permeabilized cells at Days 0 and 8, using sequential addition of substrates (for details see materials and methods), normalized to either (d) cell number (nmoles O_2/cell/min) or (e) mitochondrial mass (citrate synthase activity; nmoles O_2/cell/min/10 µmoles citrate). Values are given as mean +/− SD from three independent experiments ($n = 9$), $^*p < .05$ and $^{**}p < .01$ $^{***}p < .001$.

(co)factors involved in these processes by RT-qPCR (Supporting Information S4: Figure S4). ATAD3 KD had no effect on expression of PGC1α (a master regulator of mitochondrial biogenesis and adipogenesis), its partners NRF1/2, and the mitochondrial transcriptional factor TFAM, a PGC1α/NRF1-target gene. Thus downstream insulin signaling was undisturbed at that level, and activation of these signaling pathways during adipogenesis or any effect of ATAD3 KD on them seems to occur rather at the protein level. The situation is different for the key players that control the transcriptional cascade leading to adipocyte differentiation. While mRNA levels of C-EBPβ, an early marker of pre-adipocyte differentiation, was upregulated at Day 2 in both control and KD lines, mRNA levels of EERα, PGC1β,

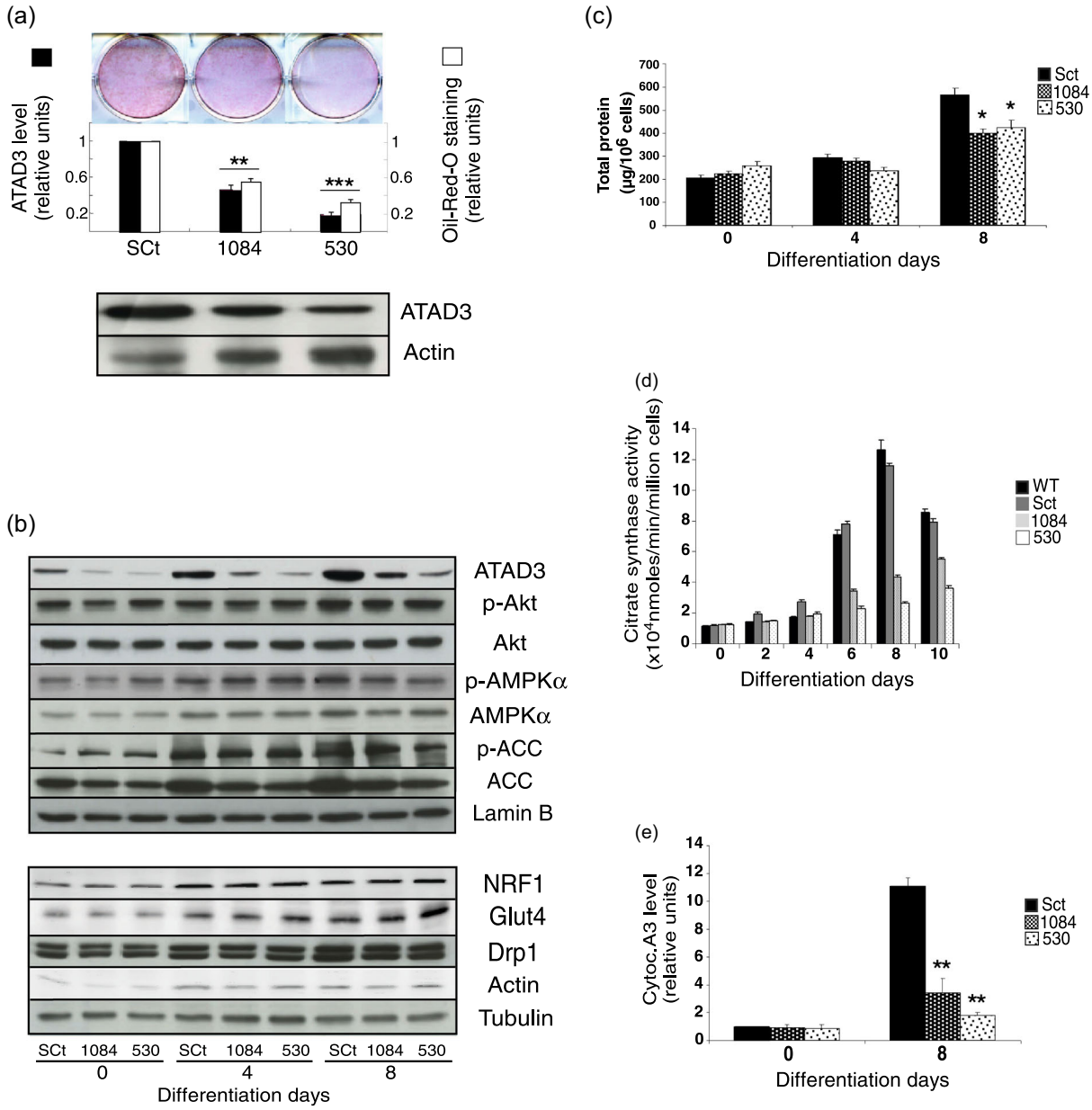

FIGURE 3 Effects of stable ATAD3 siRNA knock-down on insulin-induced differentiation of 3T3-L1 and mitochondria biogenesis 3T3-L1 scrambled siRNA control cells (SCt) were compared with stable siRNA-ATAD3 KD cell lines 1084 and 530 during the first 8 days of insulin-induced differentiation. (a) Neutral lipids quantified by Oil-Red-O staining in control and KD cells (see also Figure 3b and Supporting Information S3: S3A). Values are given as mean +/− SD from three independent experiments ($n = 9$), $^{**}p < .01$ and $^{***}p < .001$. (b) Proteins in Akt and AMPK signal transduction pathways, abundance and phosphorylation were analyzed by Western blot analysis as well as mitochondrial and differentiation-associated proteins of control (SCt), 1084 and 530 stable KD cell lines at Days 0, 4 and 8 of differentiation. Lamin B and tubulin detections were used for loading controls. (c) Total cellular protein determined by Bradford assay. Values are given as mean +/− SD from three independent experiments ($n = 9$), $^{*}p < .05$. (d) Citrate synthase activity. Values are given as mean +/− SD from three independent experiments ($n = 9$), $p < .001$ for differences between control and KD cells at day 6 and 8). (e) Respiratory chain cytochrome aa3 levels, determined by differential spectral measurement (400–650 nm) of cell lysates and using the absorbance peak at 605 nm. Values are given as mean +/− SD from three independent experiments ($n = 9$), $^{**}p < .01$.

PPARγ and C-EBPα, later markers of adipocyte differentiation, increased up to differentiation Day 7 only in control cells, but not or much less in KD cells. This indicated a block or delay of the adipogenesis program in ATAD3 KD cells already after the early differentiation steps.

3.3 | ATAD3 knock-down inhibits mitochondrial biogenesis/remodeling

We next used stable ATAD3 KD lines to analyze functional relationships between ATAD3 level and mitochondrial mass and

morphology during insulin-induced adipogenesis. Although mitochondrial mass in ATAD3 KD lines also increased continuously, it remained much lower as in control cells. Citrate synthase activity (3-5-fold; Figure 3d) and cytochrome aa3 contents (2-3-fold; Figure 3e) increased much less than in control cells (12-fold and 11-fold at Day 8, respectively). Also, expression of dynamin-related protein 1 (Drp1), a key player in mitochondrial fission and ER-mitochondria tethering processes, (de Brito & Scorrano, 2010) especially in 3T3-L1 cells, (Kita et al., 2009) was unaffected by ATAD3 KD (Figure 3b). Cytosolic markers of adipogenesis were not affected by ATAD3 KD, that is, insulin induced Glut4 and NRF1 overexpression in all cells as expected. The effect of ATAD3 KD on mitochondrial morphology was again analyzed by confocal microscopy. In constitutive ATAD3 KD lines induced to differentiate, most cells showed only limited increase of Mitotracker staining and a tubular-branched mitochondrial network, similar to undifferentiated cells, persisting throughout the entire remodeling period (Days 2–6) (Figure 4a and Supporting Information S5: Figure S5). Electron microscopy confirmed that mitochondria of insulin induced ATAD3 KD cells remain less numerous and tubular, like those of undifferentiated cells (Figure 4b). In KD cells undergoing only slight lipogenesis, we observed also recurrent accumulation of transition vesicles, probably from endoplasmic reticulum (Supporting Information S6: Figure S6A,B) with abundant enlarged granular ER and some tubular granular ER close to small lipid droplets, like in differentiating cells. Moreover, mitochondria appeared clear, with very few crests (Supporting Information S6: Figure S6C). To rule out the possibility of increased mitophagy being responsible for reduced mitochondrial mass and lipogenesis in ATAD3 KD lines, we treated the cell lines with two inhibitors of autophagy, chloroquine or bafilomycine, during the time course of insulin induction (Supporting Information S7: Figure S7B). This reduced lipogenesis to the same extend in ATAD3 KD and control cell lines, thus excluding autophagy as causative for the ATAD3 KD phenotype. Stable ATAD3 KD leading to low ATAD3 levels (line 530) reduced respiratory parameters as compared to control already before onset of differentiation (Day 0, Figure 2c). Both state III and state IV respiration (with glutamate/malate or succinate) were reduced, irrespective whether data were normalized to cell number (Figure 2c) or mitochondrial mass, i.e. citrate synthase activity (Figure 2d). Thus, below a certain threshold level of ATAD3, respiration is impaired, possibly indicating a stronger contribution of the glycolytic pathway. During differentiation (Day 8), respiration of both ATAD3 KD cell lines was clearly affected at the per cell level (Figure 2c), lacking the increase of state III and state IV respirations seen in control cells and linked to the mitochondrial mass increase. When normalized to mitochondrial mass, all respiratory parameters of KD cells decreased drastically until Day 8, including the RCR with glutamate/malate (decrease from 2.1 to 1.1), as already seen in controls (Figure 2d). However, ATAD3 KD mitochondria performed now as well as controls (with succinate) or even slightly better (with glutamate/malate).

3.4 | Rescue of ATAD3 phenotypes by ATAD3 overexpression and complementation by Drp1

To ascertain that the observed phenotype is indeed directly due to loss of ATAD3 we conducted a rescue experiment by stably transfecting the wild-type ATAD3 into the two stable ATAD3 KD cell lines. Re-expression of ATAD3 in both ATAD3 KD cell lines indeed rescued the lipogenic potential (Figure 5a) and restored mitochondrial biogenesis and remodeling (Figure 5b and Supporting Information S7: Figure S7C), with the most pronounced effect observed in line 530 which has the lowest initial ATAD3 level. We further tested the effect of stably overexpressing ATAD3 wt along with a dominant negative ATAD3 dead mutant in the original 3T3-L1 cells during differentiation. This mutant contains a nonfunctional ATPase (K358E mutation in the Walker A motif GPPGTGKT) and is dominant negative because it hetero-polymerizes with endogenous ATAD3 wt (Gilquin et al., 2010a). While stable expression of ATAD3 wt increased lipogenesis and mitochondrial biogenesis in 3T3-L1 cells induced to differentiate, expression of the dead mutant led to a significant decrease in lipogenesis and mitochondrial remodeling (Figure 5c,d). We finally hypothesized that two other mitochondrial proteins, Drp1 and Mfn2, may partially complement ATAD3 deficiency, since they are known as interactors of ATAD3 (Chiang et al., 2012; Gilquin et al., 2010b; Goller et al., 2013). Drp1 and Mfn2, involved in mitochondrial fission and fusion, respectively, where therefore overexpressed in ATAD3 KD cell lines by stable transfection. Indeed, stable overexpression of Drp1, but not of Mfn2, was able to restore lipogenesis to a variable degree in both 530 and 1084 KD cell lines (Figure 5a, b and Supporting Information S7: Figure S7C).

4 | DISCUSSION

The ubiquitous mitochondrial ATPase ATAD3 is essential during early developmental stages, as shown by knock-down in *C. elegans* (Hoffmann et al., 2009) and, more recently, in a mouse knock-out model, (Goller et al., 2013) but its precise functions are still largely unknown. Some studies have suggested a role in mitochondrial biogenesis, the maintenance of the mitochondrial network and its interaction with the endoplasmic reticulum (Fang et al., 2010; Gilquin et al., 2010b; Hoffmann et al., 2009). However, ATAD3 has not yet been implicated in any precise mitochondrial processes. Here we show by using stable and transient ATAD3 knock-down and overexpression in 3T3-L1 cells that ATAD3 plays a vital role in the adipocyte differentiation process, affecting mitochondrial mass, structure and function and lipogenesis. ATAD3 deficiency inhibits mitochondrial biogenesis, impedes changes in mitochondrial network morphology linked to Drp1 function, reduces respiration, and downregulates lipogenesis in an ACC-regulated manner. Normal insulin-induced adipogenesis in 3T3-L1 was found to involve lipogenesis, mitochondrial biogenesis and mitochondrial network fragmentation, as already established by others (Kita et al., 2009;

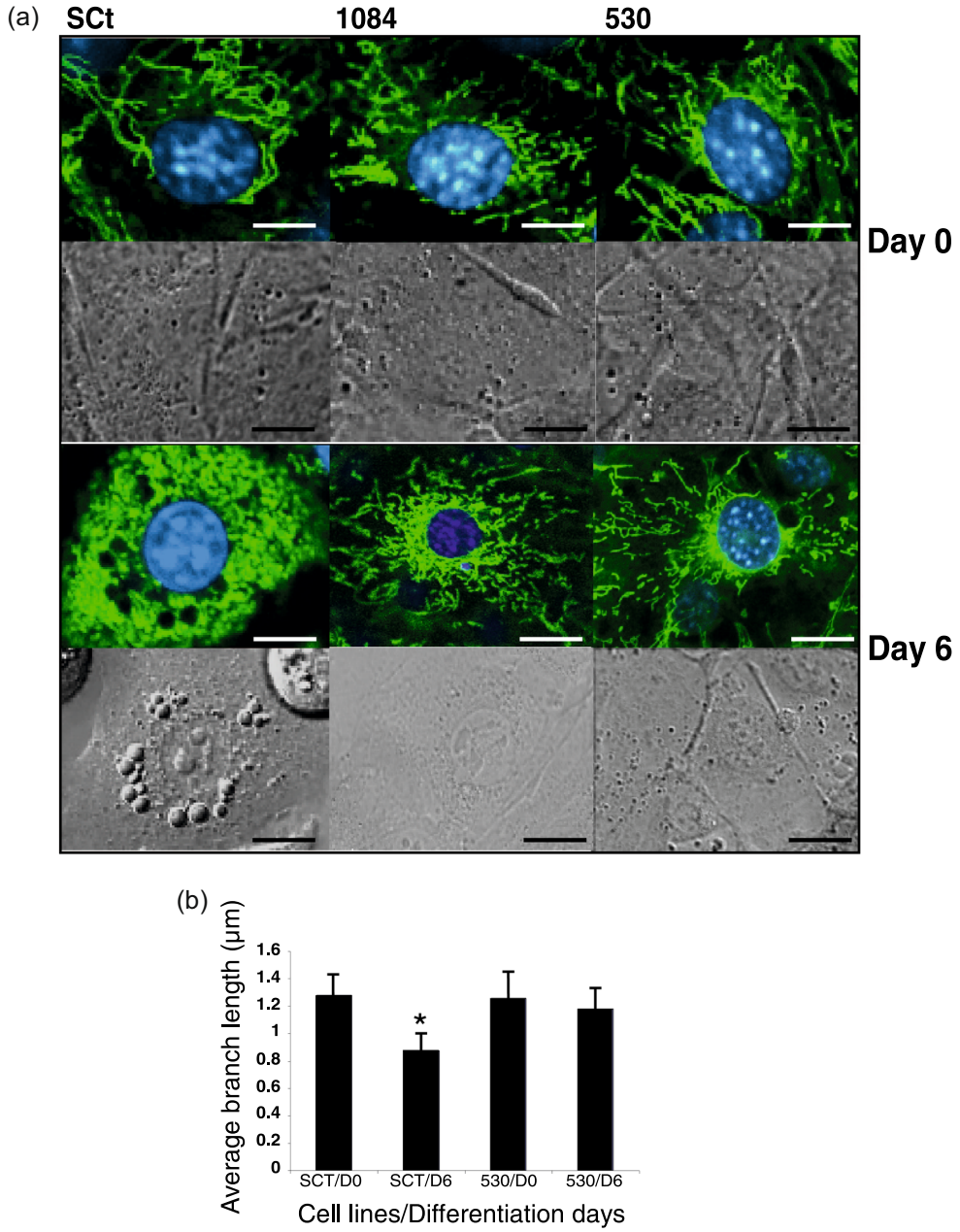

FIGURE 4 Effects of stable ATAD3 siRNA knock-down on mitochondrial remodeling. 3T3-L1 scrambled siRNA control cells (SCt) were compared with stable siRNA-ATAD3 KD cell lines 1084 and 530 during the first 6-8 days of insulin-induced differentiation. (a) Mitochondrial morphology was analyzed by confocal microscopy imaging. Confocal images (upper rows) showing typical cells stained for mitochondria (green, Mitotracker GreenFM™) and nuclei (blue, Hoechst DNA staining) together with phase contrast images (lower rows) (see also Supporting Information S6: Figure S6 for wide microscopic field imaging). Scale bars represent 5 µm. (b) Branch lengths (size) of mitochondria from 2D-analysis of electron micrographies of control (SCt) and KD cells (530) day 8 (SCt or 530 cells at day 0 present as in Figure 1f). Values are given as mean +/− SD from 981 three independent micrographs ($n = 200$), $^*p < .05$.

Wilson-Fritch et al., 2003). Importantly, upregulation of ATAD3 levels was preceding the increase of most other parameters, suggesting a role in the early differentiation program. The mitochondrial mass increase per cell was between 5 and 16-fold (abundance of different mitochondrial proteins) and 11–12-fold (based on cytochrome aa3 level and citrate synthase activity), even exceeding numbers in literature, like a 2.6-fold increase in mtDNA reported for a 3T3-L1 model or human adipose tissue (Guertin et al., 2006; McKay et al., 2003). In this respect, it is important to note that almost all literature data are normalized to total cellular protein, which increases however itself by at least threefold, while we decided to normalize to the only stable reference parameter in this system, the cell number. At this per cell level, also state IV respiration and state III respiration with succinate doubled during differentiation, as also

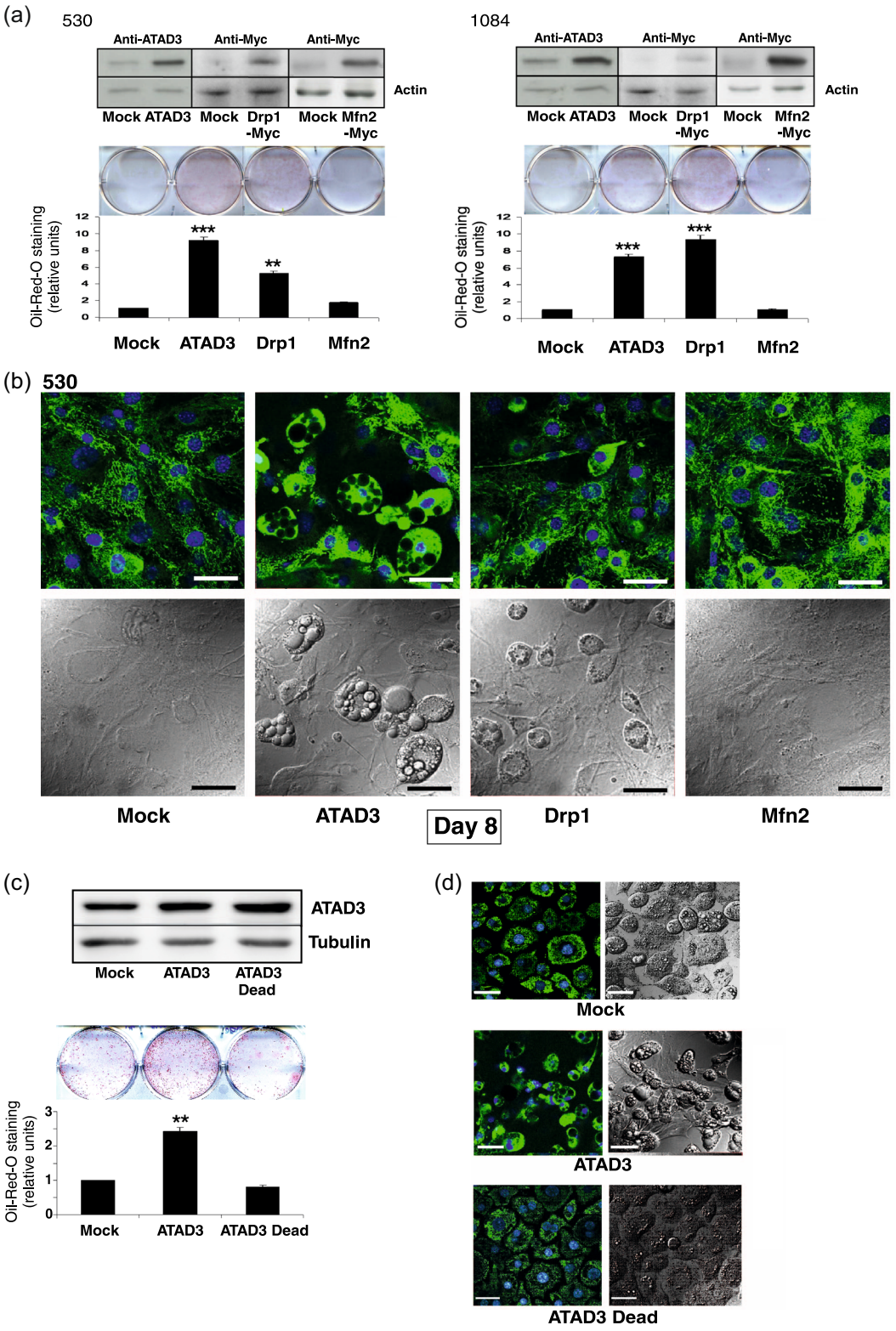

FIGURE 5 (See caption on next page).

observed earlier (Ducluzeau et al., 2011; Lu et al., 2010; Wilson-Fritch et al., 2003). However, the respiratory control ratio decreased, as did other respiratory parameters when calculated per mitochondrial mass, indicating mitochondrial uncoupling and redirection of mitochondrial metabolic activity from ATP generation towards biosynthetic activities. As seen by Antimycin lipogenic effect, triglyceride accumulation may not require so much respiration *per se*.

Functional and proteomic studies clearly suggest that during adipocyte differentiation a hyperactive TCA cycle driven by various substrates generates citrate and acetyl-CoA as precursors for triglyceride synthesis (Cho et al., 2009; Guo et al., 2008; Kajimoto et al., 2005; Newton et al., 2011). Gradual stable or transient knock-down of ATAD3 in 3T3-L1 cells led to drastic inhibition of insulin-induced adipocyte differentiation as compared to controls. This inhibition was observed at different levels, including lipogenesis, mitochondrial biogenesis and network remodeling. Consistent with these findings, overexpression of ATAD3 in 3T3-L1 cells accelerated adipogenesis, while overexpression of a dominant negative ATAD3 mutant was again inhibitory. Importantly, the 3T3-L1 KD phenotype could be rescued by re-expression of ATAD3. Thus, there exists a very close correlation between the levels of functional ATAD3 and adipogenesis, with ATAD3 representing a true limiting factor in adipogenesis. ATAD3 KD did not affect insulin-induced Akt signaling, gene expression of key transcription regulators of mitochondrial mass increase (PGC1α, NRF1, NRF2, TFAM) or of early markers of adipogenesis like C-EBPβ. We thus conclude that overall insulin signaling is intact, and that ATAD3 interferes with more downstream, mitochondria-related signaling, finally inhibiting late adipogenesis after the early stages as seen by reduced gene expression of adipogenic markers like EERα, PPARγ, PGC1β and C-EBPα. Some insulin-dependent downstream signaling is still occurring in ATAD3 KD cells, since expression of Glut4 and NRF1, two markers of adipogenesis and lipogenesis processes, is unaffected. Probably other potential activators of these genes are involved here like MEF2A, GEF, SREBP1 or CEBPβ. How ATAD3 KD can down-regulate transcription of adipogenic genes? These down regulations induced by ATAD3 KD probably reflect feed-back mechanisms. Since mitochondrial biogenesis cannot be normally increased, limiting the lipogenesis, it is expected that the adipogenic/lipogenic genetic program could be downregulated. Also and notably, ATAD3 contains a NES (Nuclear Exporting Signal) and is expressed under several isoforms (Li & Rousseau, 2012a). Therefore, ATAD3 could be itself involved in gene regulation. Also, and importantly, the adipogenic/lipogenic genetic program is only delayed by ATAD3 KD, but not blocked, thus meaning that ATAD3 is a true limiting factor in terminal adipogenesis and lipogenesis. Lipogenesis in our experimental system seems to be closely related to ACC, a rate limiting enzyme of fatty acid synthesis that switches metabolism between β-oxidation and lipogenesis (for recent reviews see (Hardie et al., 2012); Bijland et al., 2013; Ceddia, 2013). In adipocytes, the most predominant ACC isoform is ACC1, (Bianchi et al., 1990; Ha et al., 1996) which we detected, but much less is known on ACC regulation in this tissue. With 3T3-L1 cells, differentiation leads to higher ACC activity due to two effects: (i) strongly increased ACC levels, and (ii) reduced inhibitory ACC1 phosphorylation. This will accelerate lipogenesis in controls, while in ATAD3 KD cells both effects are largely diminished, thus slowing down lipogenesis. A main factor controlling ACC is AMPK, exerting negative control on ACC expression via sterol regulatory-element-binding protein-1c (SREBP-1) and ACC activity via inhibitory phosphorylation. In addition, differentiation of 3T3-L1 cells and cultured preadipocytes is inhibited by pharmacological AMPK activators (AICAR, A-769662 and many others (Habinowski & Witters, 2001); Giri et al., 2006; Vingtdeux et al., 2011; Zhou et al., 2009) or activation of AMPK upstream kinase CamKKβ (Lin et al., 2011). Such regulation may be present in 3T3-L1 controls, where covalent AMPK activation (via its T172 phosphorylation) decreases, consistent with the observed effects on ACC and lipogenesis. However, the ATAD3 KD does not affect AMPK, neither the covalent activation, nor the allosteric activation (Chen et al., 2013; Oakhill et al., 2012) as deduced from the determined adenylate ratios in control and KD cells. Probably, upregulation of transcriptional regulators like PPARγ and C-EBPα, which does not occur in KD cells, plays a major role here in controlling ACC expression, and smaller changes in phosphorylation state may be secondary to large changes in expression level. The downregulated ACC pathway in ATAD3 KD cells could be a decisive factor for decreased lipid droplet formation and reduced adipogenesis in general, although participation of increased lipolysis cannot be excluded. Besides reduced lipogenesis, the major phenotype of ATAD3 KD in 3T3-L1 cells was the inhibition of mitochondrial mass increase and remodeling. Inhibited mitochondrial biogenesis was also observed in intestinal ATAD3 KD cells in *C. elegans*, (Hoffmann et al., 2012) the functional equivalent of vertebrate adipocytes, and in case of embryonically lethal ATAD3 KO in mice, where development is early inhibited at a stage requiring mitochondrial biogenesis and ATP generation (Goller et al., 2013). Altered mitochondrial morphology and dynamics were also observed in different other cellular ATAD3 KD models (Hoffmann et al., 2012;

FIGURE 5 Effects of ATAD3 and Drp1/Mfn2 overexpressions on lipogenesis and mitochondrial remodeling. (a) Protein levels and lipogenic potential of stable ATAD3 KD cell lines 530 (left) and 1084 (right), stably transfected with ATAD3, Drp1 and Mfn2-Myc expression plasmids (and empty control vector, Mock), were determined after 12 days of insulin induction. Western blots for ATAD3, Drp1 and Myc-tagged Mfn2 are presented (top) with the quantification of neutral lipid by the Oil-red-O staining (bottom). Values are the mean +/− SD from three independent experiments ($n = 9$), $^{**}p < .01$ and $^{***}p < .001$. (b) Mitochondrial remodeling and lipogenesis in ATAD3 KD cell line 530 stably transfected with ATAD3, Drp1 and Mfn2 expression plasmids or empty vector (Mock) was analyzed at Day 8. Confocal images (top row) of cells stained for mitochondria (green, GreenFM^{TM}) and nuclei (blue, Hoechst DNA stain) together with phase contrast images (bottom row). Data obtained from 1084 cell line are presented in Supporting Information S1: Figure S8B. Scale bars represent 20μm. (c) Protein levels, lipogenic potential, and mitochondrial remodeling of wild-type 3T3-L1 cells stably transfected with ATAD3 or ATAD3 dead mutant expression plasmids (and empty vector as control, Mock) were determined after 12 days of insulin induction. Left panel: Levels of ATAD3 (analyzed by Western blot) and neutral lipids (analyzed by Oil-red-O stain and quantified). Values are given as mean +/− SD from three independent experiments ($n = 9$), $^{**}p < .01$. Right panel: Mitochondrial remodeling analyzed as in (b). Scale bars represent 20 μm.

Rone et al., 2012). This ATAD3 KD phenotype was not due to induced autophagy, since inhibition of autophagy did not increase lipogenesis as reported for hepatocytes, (Singh et al., 2009) possibly because adipocyte tissue is metabolically very different (Greenberg et al., 2011; Rosen & Spiegelman, 2006). Importantly, we show here that Drp1, a central element of the mitochondrial fission machinery, is able to complement ATAD3 KD by partially restoring mitochondrial biogenesis and also the lipogenesis that depends on the mitochondrial remodeling. This identifies Drp1 as an efficient co-factor for ATAD3 function, probably by promoting fission-based mitochondrial remodeling, (Zeller et al., 2003) consistent with earlier data on a putative interaction between ATAD3 and Drp1 (Chiang et al., 2012). These data also represent first direct evidence for a role of ATAD3 in mitochondrial remodeling and the role of this mitochondrial process in lipogenesis. ATAD3 may thus contribute to some initial fission-linked processes that trigger remodeling and biogenesis of the mitochondrial network as well as its interaction with lipid droplets (and the associated fatty acid synthesis) and the ER (and the associated local calcium signaling (de Brito & Scorrano, 2010)), all processes involving also Drp1. In support of such functional interactions, ATAD3 is targeted by calcium signaling protein S100B (Gilquin et al., 2010a) and incidentally, also, both Drp1 and ATAD3 KD increase the life span of *C. elegans* (Hoffmann et al., 2012; Yang et al., 2011). ATAD3 interacts also with another key player in mitochondrial dynamics, the fusion protein Mfn2, for importing apoptosis inducing factor (AIF), a FAD-dependent NADH oxydase, into mitochondria (Chiang et al., 2012). Finally, at the protein level, ATAD3 invalidation was reported to specifically impact mitochondrial protein synthesis (He et al., 2012). How ATAD3 KD can down-regulate abundance of mitochondrial proteins remains an open question, since some crucial transcription factors like PGC1α, NRF1, NRF2, and TFAM are not affected. Rather than transcriptional control, posttranslational processes may be involved, including protein synthesis/turnover, mitochondria/ER interactions and mitochondrial import and maturation of proteins and lipids (Schlattner et al., 2013). Indeed, most recently, ATAD3 has been shown to be involved in, and essential for cholesterol flux between ER and mitochondria compartment, especially for steroidogenesis in Leydig cells (Gerhold et al., 2015; Issop et al., 2015; Li et al., 2016; Teng et al., 2016). All these results shed the light on a possible protein/lipid transport pathway involving ATAD3 and necessary for mitochondrial biogenesis. Considering all about its major role in mitochondrial biogenesis, it is not surprising therefore that ATAD3 is a putative and strong candidate to be responsible of mutation-inherited diseases such as myopathies and neuropathies (Cooper et al., 2017; Desai et al., 2017; Eldomery et al., 2017; Harel et al., 2016).

5 | CONCLUSION

In summary, this study revealed the requirement of ATAD3 for adipocyte differentiation. First, ATAD3 is necessary for mitochondrial proliferation and remodeling. This role of ATAD3 probably involves its interaction with Drp1 that can partially compensate loss of ATAD3. Second, ATAD3 and mitochondrial biogenesis are necessary for lipogenesis and lipid droplet formation. ATAD3 seems to maintain proper mitochondrial function, despite some uncoupling and increased biosynthetic activity at the expense of ATP generation, and thus favors fatty acid synthesis via ACC and FAS. Further investigation will be necessary to understand in mechanistic detail how ATAD3 controls mitochondrial biogenesis and structural dynamics during differentiation.

ACKNOWLEDGMENTS

This work was supported by Cai Yuanpei and Xu Guangqi Hubert Curien programs from the French Ministry of Foreign affairs. We greatly thank Pr. Yao Yao and Rui Xu from the Institute of Biochemistry and Cell Biology of Shanghai Institutes for Biological Sciences Chinese Academy of Sciences for the production of ATAD3 knock-down cell lines, Sandra Pesenti from INSERM UMR-106 CarMeN laboratory for RT-PCR measurements, Morane Renoux, Maëva Ruel and Célia Bouzar for excellent technical assistance in cell culture and Western blot experiments, Stéphane Attia for nucleotide analysis, and Frédéric Lamarche for perfect supervision of cell culture facilities. We thank very much Karin Pernet-Gallay and Julie Delaroche for their excellent expertises in electronic microscopy analysis and Cécile Cottet- Rousselle for accompaniment in confocal microscopy. We are also grateful to Pr. Valdur Saks and Dr. Rita Guzun for their essential advices in the expending field of mitochondria research.

CONFLICT OF INTEREST STATEMENT

The authors declare that they have no conflict of interest.

DATA AVAILABILITY STATEMENT

The authors state that all data are available upon request to D.R. by email communication.

ORCID

Denis Rousseau http://orcid.org/0000-0001-9322-4406

REFERENCES

Arguello, T., Peralta, S., Antonicka, H., Gaidosh, G., Diaz, F., Tu, Y. T., Garcia, S., Shiekhattar, R., Barrientos, A., & Moraes, C. T. (2021). ATAD3A has a scaffolding role regulating mitochondria inner membrane structure and protein assembly. *Cell Reports*, *37*(12), 110139.

Baudier, J. (2018). ATAD3 proteins: Brokers of a mitochondria-endoplasmic reticulum connection in mammalian cells. *Biological Reviews*, *93*(2), 827–844.

Bianchi, A., Evans, J. L., Iverson, A. J., Nordlund, A. C., Watts, T. D., & Witters, L. A. (1990). Identification of an isozymic form of acetyl-CoA carboxylase. *Journal of Biological Chemistry*, *265*, 1502–1509.

Bijland, S., Mancini, S. J., & Salt, I. P. (2013). Role of AMP-activated protein kinase in adipose tissue metabolism and inflammation. *Clinical Science*, *124*, 491–507. https://doi.org/10.1042/CS20120536

Blanchette-Mackie, E. J., Dwyer, N. K., Barber, T., Coxey, R. A., Takeda, T., Rondinone, C. M., Theodorakis, J. L., Greenberg, A. S., & Londos, C.

(1995). Perilipin is located on the surface layer of intracellular lipid droplets in adipocytes. *Journal of Lipid Research*, *36*, 1211–1226.

Bogacka, I., Ukropcova, B., McNeil, M., Gimble, J. M., & Smith, S. R. (2005). Structural and functional consequences of mitochondrial biogenesis in human adipocytesin vitro. *The Journal of Clinical Endocrinology & Metabolism*, *90*, 6650–6656.

Bogenhagen, D. F., Rousseau, D., & Burke, S. (2008). The layered structure of human mitochondrial DNA nucleoids. *Journal of Biological Chemistry*, *283*, 3665–3675.

de Brito, O. M., & Scorrano, L. (2008). Mitofusin 2 tethers endoplasmic reticulum to mitochondria. *Nature*, *456*, 605–610.

de Brito, O. M., & Scorrano, L. (2010). An intimate liaison: Spatial organization of the endoplasmic reticulum-mitochondria relationship. *The EMBO Journal*, *29*, 2715–2723.

Campello, S., & Scorrano, L. (2010). Mitochondrial shape changes: Orchestrating cell pathophysiology. *EMBO Reports*, *11*, 678–684.

Ceddia, R. B. (2013). The role of AMP-activated protein kinase in regulating white adipose tissue metabolism. *Molecular and Cellular Endocrinology*, *366*, 194–203. https://doi.org/10.1016/j.mce.2012.06.014

Chen, L., Xin, F. J., Wang, J., Hu, J., Zhang, Y. Y., Wan, S., Cao, L. S., Lu, C., Li, P., Yan, S. F., Neumann, D., Schlattner, U., Xia, B., Wang, Z. X., & Wu, J. W. (2013). Conserved regulatory elements in AMPK. *Nature*, *498*, E8–E10. https://doi.org/10.1038/nature12189

Chen, T. C., Hung, Y. C., Lin, T. Y., Chang, H. W., Chiang, I. P., Chen, Y. Y., & Chow, K. C. (2011). Human papillomavirus infection and expression of ATPase family AAA domain containing 3A, a novel anti-autophagy factor, in uterine cervical cancer. *International Journal of Molecular Medicine*, *28*, 689–696.

Chiang, S. F., Huang, C. Y., Lin, T. Y., Chiou, S. H., & Chow, K. C. (2012). An alternative import pathway of AIF to the mitochondria. *International Journal of Molecular Medicine*, *29*, 365–372.

Cho, S. Y., Park, P. J., Shin, E. S., Lee, J. H., Chang, H. K., & Lee, T. R. (2009). Proteomic analysis of mitochondrial proteins of basal and lipolytically (isoproterenol and TNF-α)-stimulated adipocytes. *Journal of Cellular Biochemistry*, *106*, 257–266.

Choo, H. J., Kim, J. H., Kwon, O. B., Lee, C. S., Mun, J. Y., Han, S. S., Yoon, Y. S., Yoon, G., Choi, K. M., & Ko, Y. G. (2006). Mitochondria are impaired in the adipocytes of type 2 diabetic mice. *Diabetologia*, *49*, 784–791.

Cooper, H. M., Yang, Y., Ylikallio, E., Khairullin, R., Woldegebriel, R., Lin, K. L., Euro, L., Palin, E., Wolf, A., Trokovic, R., Isohanni, P., Kaakkola, S., Auranen, M., Lönnqvist, T., Wanrooij, S., & Tyynismaa, H. (2017). ATPase-deficient mitochondrial inner membrane protein ATAD3A disturbs mitochondrial dynamics in dominant hereditary spastic paraplegia. *Human Molecular Genetics*, *26*(8), 1432–1443. https://doi.org/10.1093/hmg/ddx042

Da Cruz, S., & Martinou, J. C. (2008). Purification and proteomic 721 analysis of the mouse liver mitochondrial inner membrane. *Methods in Molecular Biology*, *432*, 101–116.

Da Cruz, S., Xenarios, I., Langridge, J., Vilbois, F., Parone, P. A., & Martinou, J. C. (2003). Proteomic analysis of the mouse liver mitochondrial inner membrane. *Journal of Biological Chemistry*, *278*, 41566–41571.

Csordás, G., Renken, C., Várnai, P., Walter, L., Weaver, D., Buttle, K. F., Balla, T., Mannella, C. A., & Hajnóczky, G. (2006). Structural and functional features and significance of the physical linkage between ER and mitochondria. *The Journal of Cell Biology*, *174*, 915–921.

Desai, R., Frazier, A. E., Durigon, R., Patel, H., Jones, A. W., Dalla Rosa, I., Lake, N. J., Compton, A. G., Mountford, H. S., Tucker, E. J., Mitchell, A. L. R., Jackson, D., Sesay, A., Di Re, M., van den Heuvel, L. P., Burke, D., Francis, D., Lunke, S., McGillivray, G., … Spinazzola, A. (2017). ATAD3 gene cluster deletions cause cerebellar dysfunction associated with altered mitochondrial DNA and cholesterol metabolism. *Brain*, *140*(6), 1595–1610. https://doi.org/10.1093/brain/awx094

Ducluzeau, P. H., Priou, M., Weitheimer, M., Flamment, M., Duluc, L., Iacobazi, F., Soleti, R., Simard, G., Durand, A., Rieusset, J., Andriantsitohaina, R., & Malthièry, Y. (2011). Dynamic regulation of mitochondrial network and oxidative functions during 3T3-L1 fat cell differentiation. *Journal of Physiology and Biochemistry*, *67*, 285–296.

Eldomery, M. K., Coban-Akdemir, Z., Harel, T., Rosenfeld, J. A., Gambin, T., Stray-Pedersen, A., Küry, S., Mercier, S., Lessel, D., Denecke, J., Wiszniewski, W., Penney, S., Liu, P., Bi, W., Lalani, S. R., Schaaf, C. P., Wangler, M. F., Bacino, C. A., Lewis, R. A., … Lupski, J. R. (2017). Lessons learned from additional research analyses of unsolved clinical exome cases. *Genome Medicine*, *9*(1), 26. https://doi.org/10.1186/s13073-017-0412-6

Epand, R. F., Tokarska-Schlattner, M., Schlattner, U., Wallimann, T., & Epand, R. M. (2007). Cardiolipin clusters and membrane domain formation induced by mitochondrial proteins. *Journal of Molecular Biology*, *365*, 968–980.

Fang, H. Y., Chang, C. L., Hsu, S. H., Huang, C. Y., Chiang, S. F., Chiou, S. H., Huang, C. H., Hsiao, Y. T., Lin, T. Y., Chiang, I. P., Hsu, W. H., Sugano, S., Chen, C. Y., Lin, C. Y., Ko, W. J., & Chow, K. C. (2010). ATPase family AAA domain-containing 3A is a novel anti-apoptotic factor in lung adenocarcinoma cells. *Journal of Cell Science*, *123*, 1171–1180.

Frayn, K. N., Arner, P., & Yki-Järvinen, H. (2006). Fatty acid metabolism in adipose tissue, muscle and liver in health and disease. *Essays in Biochemistry*, *42*, 89–103.

Gao, C. L., Liu, G. L., Liu, S., Chen, X. H., Ji, C. B., Zhang, C. M., Xia, Z. K., & Guo, X. (2011). Overexpression of PGC-1β improves insulin sensitivity and mitochondrial function in 3T3- L1 adipocytes. *Molecular and Cellular Biochemistry*, *353*, 215–223.

Gerhold, J. M., Cansiz-Arda, Ş., Lõhmus, M., Engberg, O., Reyes, A., van Rennes, H., Sanz, A., Holt, I. J., Cooper, H. M., & Spelbrink, J. N. (2015). Human mitochondrial DNA-protein complexes attach to a cholesterol-rich membrane structure. *Scientific Reports*, *5*, 15292. https://doi.org/10.1038/srep15292

Gilquin, B., Cannon, B. R., Hubstenberger, A., Moulouel, B., Falk, E., Merle, N., Assard, N., Kieffer, S., Rousseau, D., Wilder, P. T., Weber, D. J., & Baudier, J. (2010a). The calcium dependent interaction between S100B and the mitochondrial AAA ATPase ATAD3A and the role of this complex in the cytoplasmic processing of ATAD3A. *Molecular and Cellular Biology*, *30*, 2724–2736.

Gilquin, B., Taillebourg, E., Cherradi, N., Hubstenberger, A., Gay, O., Merle, N., Assard, N., Fauvarque, M. O., Tomohiro, S., Kuge, O., & Baudier, J. (2010b). The AAA+ ATPase ATAD3A controls mitochondrial dynamics at the interface of the inner and outer membrane. *Molecular and Cellular Biology*, *30*, 1984–1996.

Gires, O., Münz, M., Schaffrik, M., Kieu, C., Rauch, J., Ahlemann, M., Eberle, D., Mack, B., Wollenberg, B., Lang, S., Hofmann, T., Hammerschmidt, W., & Zeidler, R. (2004). Profile identification of disease-associated humoral antigens using AMIDA, a novel proteomics-based technology. *Cellular and Molecular Life Sciences (CMLS)*, *61*, 1198–1207.

Giri, S., Rattan, R., Haq, E., Khan, M., Yasmin, R., Won, J., Key, L., Singh, A. K., & Singh, I. (2006). AICAR inhibits adipocyte differentiation in 3T3L1 and restores metabolic alterations in diet- induced obesity mice model. *Nutrition & Metabolism*, *3*, 31.

Goetz, J. G., Genty, H., St-Pierre, P., Dang, T., Joshi, B., Sauvé, R., Vogl, W., & Nabi, I. R. (2007). Reversible interactions between smooth domains of the endoplasmic reticulum and mitochondria are regulated by physiological cytosolic Ca2+ levels. *Journal of Cell Science*, *120*, 3553–3564.

Goller, T., Seibold, U. K., Kremmer, E., Voos, W., & Kolanus, W. (2013). Atad3 function is essential for early post-implantation development in the mouse. *PLoS One*, *8*, e54799. https://doi.org/10.1371/journal.pone.0054799

Goodman, J. M. (2008). The gregarious lipid droplet. *Journal of Biological Chemistry*, *283*, 28005–28009.

Gratia, S., Kay, L., Potenza, L., Seffouh, A., Novel-Chaté, V., Schnebelen, C., Sestili, P., Schlattner, U., & Tokarska-Schlattner, M. (2012). Inhibition of AMPK signalling by doxorubicin: at the crossroads of the cardiac responses to energetic, oxidative, and genotoxic stress. *Cardiovascular Research*, *95*, 290–299.

Greenberg, A. S., Coleman, R. A., Kraemer, F. B., McManaman, J. L., Obin, M. S., Puri, V., Yan, Q. W., Miyoshi, H., & Mashek, D. G. (2011). The role of lipid droplets in metabolic disease in rodents and humans. *Journal of Clinical Investigation*, *121*, 2102–2110.

Guertin, D. A., Guntur, K. V. P., Bell, G. W., Thoreen, C. C., & Sabatini, D. M. (2006). Functional genomics identifies TOR-regulated genes that control growth and division. *Current Biology*, *16*, 958–970.

Guo, Y., Cordes, K. R., Farese, R. V., & Walther, Jr. TC. (2009). Lipid droplets at a glance. *Journal of Cell Science*, *122*, 749–752.

Guo, Y., Walther, T. C., Rao, M., Stuurman, N., Goshima, G., Terayama, K., Wong, J. S., Vale, R. D., Walter, P., & Farese, R. V. (2008). Functional genomic screen reveals genes involved in lipid- droplet formation and utilization. *Nature*, *453*, 657–661.

Ha, J., Lee, J. K., Kim, K. S., Witters, L. A., & Kim, K. H. (1996). Cloning of human acetyl- CoA carboxylase-beta and its unique features. *Proceedings of the National Academy of Sciences*, *93*, 11466–11470.

Habinowski, S. A., & Witters, L. A. (2001). The effects of AICAR on adipocyte differentiation of 3T3-L1 cells. *Biochemical and Biophysical Research Communications*, *286*, 852–856.

Hardie, D. G., Ross, F. A., & Hawley, S. A. (2012). AMPK: A nutrient and energy sensor that maintains energy homeostasis. *Nature Reviews Molecular Cell Biology*, *13*, 251–262. https://doi.org/10.1038/nrm3311

Harel, T., Yoon, W. H., Garone, C., Gu, S., Coban-Akdemir, Z., Eldomery, M. K., Posey, J. E., Jhangiani, S. N., Rosenfeld, J. A., Cho, M. T., Fox, S., Withers, M., Brooks, S. M., Chiang, T., Duraine, L., Erdin, S., Yuan, B., Shao, Y., Moussallem, E., … Lupski, J. R. (2016). Recurrent de novo and biallelic variation of ATAD3A, encoding a mitochondrial membrane protein, results in distinct neurological syndromes. *The American Journal of Human Genetics*, Oct 6 *99*(4), 831–845. https://doi.org/10.1016/j.ajhg.2016.08.007

He, J., Cooper, H. M., Reyes, A., Di Re, M., Sembongi, H., Litwin, T. R., Gao, J., Neuman, K. C., Fearnley, I. M., Spinazzola, A., Walker, J. E., & Holt, I. J. (2012). Mitochondrial nucleoid interacting proteins support mitochondrial protein synthesis. *Nucleic Acids Research*, *40*, 6109–6121.

Hoffmann, M., Bellance, N., Rossignol, R., Koopman, W. J. H., Willems, P. H. G. M., Mayatepek, E., Bossinger, O., & Distelmaier, F. (2009). *C. elegans* ATAD-3 is essential for mitochondrial activity and development. *PLoS One*, *4*, e7644.

Hoffmann, M., Honnen, S., Mayatepek, E., Wätjen, W., Koopman, W. J. H., Bossinger, O., & Distelmaier, F. (2012). MICS-1 interacts with mitochondrial ATAD-3 and modulates lifespan in *C. elegans*. *Experimental Gerontology*, *47*, 270–275.

Huang, K. H., Chow, K. C., Chang, H. W., Lin, T. Y., & Lee, M. C. (2011). The ATPase family, AAA domain containing 3A is an anti-apoptotic factor and a secretion regulator of PSA in the prostate cancer. *International Journal of Molecular Medicine*, *28*, 9–15.

Hubstenberger, A., Labourdette, G., Baudier, J., & Rousseau, D. (2008). ATAD3A and ATAD3B are distal 1p-located genes differentially expressed in human glioma cell lines and present in vitro anti-oncogenic and chemoresistant properties. *Experimental Cell Research*, *314*, 2870–2883.

Hubstenberger, A., Merle, N., Charton, R., Brandolin, G., & Rousseau, D. (2010). Topological analysis of ATAD3A insertion in purified human mitochondria. *Journal of Bioenergetics and Biomembranes*, *42*, 143–150.

Issop, L., Fan, J., Lee, S., Rone, M. B., Basu, K., Mui, J., & Papadopoulos, V. (2015). Mitochondria- associated membrane formation in hormone-stimulated Leydig cell steroidogenesis: role of ATAD3. *Endocrinology*, *156*(1), 334–345. https://doi.org/10.1210/en.2014-1503

Kaaman, M., Sparks, L. M., van Harmelen, V., Smith, S. R., Sjölin, E., Dahlman, I., & Arner, P. (2007). Strong association between mitochondrial DNA copy number and lipogenesis in human white adipose tissue. *Diabetologia*, *50*, 2526–2533.

Kageyama, Y., Zhang, Z., & Sesaki, H. (2011). Mitochondrial division: Molecular machinery and physiological functions. *Current Opinion in Cell Biology*, *23*, 427–434.

Kajimoto, K., Terada, H., Baba, Y., & Shinohara, Y. (2005). Essential role of citrate export from mitochondria at early differentiation stage of 3T3-L1 cells for their effective differentiation into fat cells, as revealed by studies using specific inhibitors of mitochondrial di- and tricarboxylate carriers. *Molecular Genetics and Metabolism*, *85*, 46–53.

Kamath, R. (2003). Genome-wide RNAi screening in *Caenorhabditis elegans*. *Methods*, *30*, 313–321.

Kazantzis, M., & Stahl, A. (2012). Fatty acid transport proteins, implications in physiology and disease. *Biochimica et Biophysica Acta (BBA) - Molecular and Cell Biology of Lipids*, *1821*, 852–857.

Kita, T., Nishida, H., Shibata, H., Niimi, S., Higuti, T., & Arakaki, N. (2009). Possible role of mitochondrial remodelling on cellular triacylglycerol accumulation. *Journal of Biochemistry*, *146*, 787–796.

Lee, H., & Kim, D. W. (2022). Deletion of ATAD3A inhibits osteogenesis by impairing mitochondria structure and function in pre-osteoblast. *Developmental Dynamics*, *251*(12), 1982–2000.

Li, S., Bouzar, C., Cottet-Rousselle, C., Zagotta, I., Lamarche, F., Wabitsch, M., Tokarska- Schlattner, M., Fischer-Posovszky, P., Schlattner, U., & Rousseau, D. (2016). Resveratrol inhibits lipogenesis of 3T3-L1 and SGBS cells by inhibition of insulin signaling and mitochondrial mass increase. *Biochimica et Biophysica Acta (BBA) - Bioenergetics*, *1857*(6), 643–652. https://doi.org/10.1016/j.bbabio.2016.03.009

Li, S., Clémençon, B., Catty, C., Brandolin, B., Schlattner, U., & Rousseau, D. (2012b). Yeast- based production and purification of HIS-tagged human ATAD3A, a specific target of S100B. *Protein Expression and Purification*, *83*, 211–216.

Li, S., & Rousseau, D. (2012a). ATAD3, a vital membrane bound 692 mitochondrial ATPase involved in tumor progression. *Journal of Biobased Materials and Bioenergy 44*, 189–197.

Lin, F., Ribar, T. J., & Means, A. R. (2011). The Ca2+/calmodulin-dependent protein kinase kinase, CaMKK2, inhibits preadipocyte differentiation. *Endocrinology*, *152*, 3668–3679. https://doi.org/10.1210/en.2011-1107

Lu, R., Ji, H., Chang, Z., Su, S., & Yang, G. (2010). Mitochondrial development and the influence of its dysfunction during rat adipocyte differentiation. *Molecular Biology Reports*, *37*, 2173–2182.

McKay, R. M., McKay, J. P., Avery, L., & Graff, J. M. (2003). C. elegans. *Developmental Cell*, *4*, 131–142.

Miller, W. L. (2011). Role of mitochondria in steroidogenesis. *Endocrine Development*, *20*, 1–19.

Monge, C., Beraud, N., Kuznetsov, A. V., Rostovtseva, T., Sackett, D., Schlattner, U., Vendelin, M., & Saks, V. A. (2008). Regulation of respiration in brain mitochondria and synaptosomes: Restrictions of ADP diffusion in situ, roles of tubulin, and mitochondrial creatine kinase. *Molecular and Cellular Biochemistry*, *318*, 147–165.

Muoio, D. M., Seefeld, K., Witters, L. A., & Coleman, R. A. (1999). AMP-activated kinase reciprocally regulates triacylglycerol synthesis and fatty acid oxidation in liver and muscle: Evidence that *sn*-glycerol-3-phosphate acyltransferase is a novel target. *Biochemical Journal*, *338*, 783–791.

Newton, B. W., Cologna, S. M., Moya, C., Russell, D. H., Russell, W. K., & Jayaraman, A. (2011). Proteomic analysis of 3T3-L1 adipocyte mitochondria during differentiation and enlargement. *Journal of Proteome Research*, *10*, 4692–4702.

Novikoff, A. B., Novikoff, P. M., Rosen, O. M., & Rubin, C. S. (1980). Organelle relationships in cultured 3T3-L1 preadipocytes. *The Journal of Cell Biology*, *87*, 180–196.

Oakhill, J. S., Scott, J. W., & Kemp, B. E. (2012). AMPK functions as an adenylate charge regulated protein kinase. *Trends in Endocrinology & Metabolism*, *23*, 125–132. https://doi.org/10.1016/j.tem.2011.12.006

Osman, C., Voelker, D. R., & Langer, T. (2011). Making heads or tails of phospholipids in mitochondria. *Journal of Cell Biology*, *192*, 7–16.

Peralta, S., Goffart, S., Williams, S. L., Diaz, F., Garcia, S., Nissanka, N., Area -Gomez, E., Pohjoismäki, J., & Moraes, C. T. (2018). ATAD3 controls mitochondrial cristae structure in mouse muscle, influencing mtDNA replication and cholesterol levels. *Journal of Cell Science*, *131*(13), jcs217075.

Piano, F., Schetter, A. J., Morton, D. G., Gunsalus, K. C., Reinke, V., Kim, S. K., & Kemphues, K. J. (2002). Gene clustering based on RNAi phenotypes of ovary-enriched genes in *C. elegans*. *Current Biology*, *12*, 1959–1964.

Rone, M. B., Midzak, A. S., Issop, L., Rammouz, G., Jagannathan, S., Fan, J., Ye, X., Blonder, J., Veenstra, T., & Papadopoulos, V. (2012). Identification of a dynamic mitochondrial protein complex driving cholesterol import, trafficking, and metabolism to steroid hormones. *Molecular Endocrinology*, *26*, 1868–1882. https://doi.org/10.1210/me.2012-1159

Rosen, E. D., & Spiegelman, B. M. (2006). Adipocytes as regulators of energy balance and glucose homeostasis. *Nature*, *444*, 847–853.

Schaffrik, M., Mack, B., Matthias, C., Rauch, J., & Gires, O. (2006). Molecular characterization of the tumor-associated antigen AAA-TOB3. *Cellular and Molecular Life Sciences*, *63*, 2162–2174.

Schlattner, U., Tokarska-Schlattner, M., Rousseau, D., Boissan, M., Mannella, C., Epand, R., & Lacombe, M. L. (2013). Mitochondrial cardiolipin/phospholipid trafficking: The role of membrane contact site complexes and lipid transfer proteins. *Chemistry and Physics of Lipids*, *179*, 32–41. https://doi.org/10.1016/j.chemphyslip.2013.12.008

Shi, Y., & Burn, P. (2004). Lipid metabolic enzymes: Emerging drug targets for the treatment of obesity. *Nature Reviews Drug Discovery*, *3*, 695–71052.

Shu, L., Hu, C., Xu, M., Yu, J., He, H., Lin, J., Sha, H., Lu, B., Engelender, S., Guan, M., & Song, Z. (2021). ATAD3B is a mitophagy receptor mediating clearance of oxidative stress-induced damaged mitochondrial DNA. *EMBO Journal*, *40*(8), e106283.

Simmer, F., Moorman, C., van der Linden, A. M., Kuijk, E., van den Berghe, P. V. E., Kamath, R. S., Fraser, A. G., Ahringer, J., & Plasterk, R. H. A. (2003). Genome-wide RNAi of *C. elegans* using the hypersensitive rrf-3 strain reveals novel gene functions. *PLoS Biology*, *1*, e12.

Singh, R., Kaushik, S., Wang, Y., Xiang, Y., Novak, I., Komatsu, M., Tanaka, K., Cuervo, A. M., & Czaja, M. J. (2009). Autophagy regulates lipid metabolism. *Nature*, *458*, 1131–1135.

Sönnichsen, B., Koski, L. B., Walsh, A., Marschall, P., Neumann, B., Brehm, M., Alleaume, A. M., Artelt, J., Bettencourt, P., Cassin, E., Hewitson, M., Holz, C., Khan, M., Lazik, S., Martin, C., Nitzsche, B., Ruer, M., Stamford, J., Winzi, M., … Echeverri, C. J. (2005). Full-genome RNAi profiling of early embryogenesis in *Caenorhabditis elegans*. *Nature*, *434*, 462–469.

Suter, M., Riek, U., Tuerk, R., Schlattner, U., Wallimann, T., & Neumann, D. (2006). Dissecting the role of 5'-AMP for allosteric stimulation, activation, and deactivation of AMP-activated protein kinase. *Journal of Biological Chemistry*, *281*, 32207–32216.

Szabadkai, G., Bianchi, K., Várnai, P., De Stefani, D., Wieckowski, M. R., Cavagna, D., Nagy, I., Balla, T., & Rizzuto, R. (2006). Chaperone-mediated coupling of endoplasmic reticulum and mitochondrial Ca2+ channels. *The Journal of Cell Biology*, *175*, 901–911.

Teng, Y., Ren, X., Li, H., Shull, A., Kim, J., & Cowell, J. K. (2016). Mitochondrial ATAD3A combines with GRP78 to regulate the WASF3 metastasis-promoting protein. *Oncogene*, *35*(3), 333–343. https://doi.org/10.1038/onc.2015.86

Vance, J. E. (2008). Thematic review series: Glycerolipids. phosphatidylserine and phosphatidylethanolamine in mammalian cells: Two metabolically related aminophospholipids. *Journal of Lipid Research*, *49*, 1377–1387.

Vankoningsloo, S., Piens, M., Lecocq, C., Gilson, A., De Pauw, A., Renard, P., Demazy, C., Houbion, A., Raes, M., & Arnould, T. (2005). Mitochondrial dysfunction induces triglyceride accumulation in 3T3-L1 cells: Role of fatty acid β-oxidation and glucose. *Journal of Lipid Research*, *46*, 1133–1149.

Vingtdeux, V., Chandakkar, P., Zhao, H., Davies, P., & Marambaud, P. (2011). Small-Molecule activators of AMP-activated protein kinase (AMPK), RSVA314 and RSVA405, inhibit adipogenesis. *Molecular Medicine*, *17*, 1022–1030.

Voelker, D. R. (2003). New perspectives on the regulation of intermembrane glycerophospholipid traffic. *Journal of Lipid Research*, *44*, 441–449.

Walther, T. C., & Farese, R. V. (2009). The life of lipid droplets. *Biochimica et Biophysica Acta (BBA) - Molecular and Cell Biology of Lipids*, *1791*, 459–466.

Wang, H. J., Guay, G., Pogan, L., Sauvé, R., & Nabi, I. R. (2000). Calcium regulates the association between mitochondria and a smooth subdomain of the endoplasmic reticulum. *The Journal of Cell Biology*, *150*, 1489–1498.

Westermann, B. (2010). Mitochondrial fusion and fission in cell life and death. *Nature Reviews Molecular Cell Biology*, *11*, 872–884.

Wilson-Fritch, L., Burkart, A., Bell, G., Mendelson, K., Leszyk, J., Nicoloro, S., Czech, M., & Corvera, S. (2003). Mitochondrial biogenesis and remodeling during adipogenesis and in response to the insulin sensitizer rosiglitazone. *Molecular and Cellular Biology*, *23*, 1085–1094.

Xie, W., Hamilton, J. A., Kirkland, J. L., Corkey, B. E., & Guo, W. (2006). Oleate-induced formation of fat cells with impaired insulin sensitivity. *Lipids*, *41*, 267–271.

Yang, C. C., Chen, D., Lee, S. S., & Walter, L. (2011). The dynamin-related protein DRP-1 and the insulin signaling pathway cooperate to modulate *Caenorhabditis elegans* longevity. *Aging cell*, *10*, 724–728.

Zeller, K. I., Jegga, A. G., Aronow, B. J., O'Donnell, K. A., & Dang, C. V. (2003). An integrated database of genes responsive to the Myc oncogenic transcription factor: Identification of direct genomic targets. *Genome Biology*, *4*:R69.

Zhou, Y., Wang, D., Zhu, Q., Gao, X., Yang, S., Xu, A., & Wu, D. (2009). Inhibitory effects of A-769662, a novel activator of AMP-activated protein kinase, on 3T3-L1 adipogenesis. *Biological and Pharmaceutical Bulletin*, *32*, 993–998.

SUPPORTING INFORMATION

Additional supporting information can be found online in the Supporting Information section at the end of this article.

How to cite this article: Li, S., Xu, R., Yao, Y., & Rousseau, D. (2024). ATAD3 is a limiting factor in mitochondrial biogenesis and adipogenesis of white adipocyte-like 3T3-L1 cells. *Cell Biology International*, 1–17. https://doi.org/10.1002/cbin.12206